

THE UNIVERSITY OF MICHIGAN
ANN ARBOR, MICHIGAN

QUARTERLY PROGRESS REPORT NO. 6

FOR

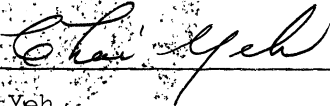
BASIC RESEARCH IN MICROWAVE DEVICES AND QUANTUM ELECTRONICS

This report covers the period August 1, 1964 to November 1, 1964

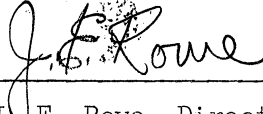
Electron Physics Laboratory
Department of Electrical Engineering

By: H. K. Detweiler
M. E. El-Shandwily
B. Ho
J. E. Rowe
C. Yeh

Approved by:


C. Yeh
Project Engineer

Approved by:


J. E. Rowe, Director
Electron Physics Laboratory

Project 05772

DEPARTMENT OF THE NAVY
BUREAU OF SHIPS
WASHINGTON 25, D. C.
PROJECT SERIAL NO. SR0080301, TASK 9391
CONTRACT NO. Nobsr-89274

November, 1964

21571

MRC567

v. 6

ABSTRACT

Equations for the modulation products in the multi-signal analysis of an amplitude- and phase-modulated traveling-wave amplifier have been programmed and the results computed. The computation includes all three theoretical approaches derived and discussed in previous reports. These include the nonlinear approach using the two-signal input, the large-signal analysis using the multiple signal input and the Boltzmann transport equation approach using the multiple signal input. The output powers of some important cross-modulation components, the cross-modulation factors, etc. are presented in graphs. Experimental results using two and three signal inputs are presented for comparison.

A large-signal analysis is carried out for a d-c pumped quadrupole amplifier employing cyclotron-synchronous wave interaction. Criteria for the validity of small-signal and large-signal analyses are established by means of the phase slip. Energy relations between the beam and the pumping field are discussed for a strong pumping field condition that would lead to the anomalous gain possibility.

The technique for insertion of the helix-BeO rod into a metal envelope to improve the thermal conductivity of the assembly is developed.

TABLE OF CONTENTS

	<u>Page</u>
ABSTRACT	iii
LIST OF ILLUSTRATIONS	vi
PERSONNEL	viii
1. GENERAL INTRODUCTION	1
2. GENERATION AND AMPLIFICATION OF COHERENT ELECTROMAGNETIC ENERGY IN THE MILLIMETER AND SUBMILLIMETER WAVELENGTH REGION	2
2.1 Study of Frequency Multiplication in an Angular Propagating Circuit	2
2.2 Investigation of High-Thermal-Conductivity Materials for Devices Above X-Band	2
2.2.1 Introduction	2
2.2.2 Experimental Effort	2
2.2.3 Future Work	3
3. ANALYSIS OF AMPLITUDE- AND PHASE-MODULATED TRAVELING-WAVE AMPLIFIERS	4
3.1 Introduction	4
3.2 Results.	4
3.2.1 Theoretical Results from the Integration of Equations of Motion Method	4
3.2.2 Boltzmann Transport Equation Method	15
3.2.3 Experimental Work	15
3.2.4 Large-Signal Analysis	22
3.3 Future Work	23
4. STUDY OF A D-C PUMPED QUADRUPOLE AMPLIFIER	23
4.1 Introduction	23
4.2 Large-Signal Analysis of Quadrifilar D-c Pump Cyclotron-Synchronous Wave Quadrupole Amplifier	24
4.2.1 Assumptions for the Analysis	24
4.2.2 The Axial Beam Velocity and Phase Slip	24
4.2.3 Potential Distribution of the Pump Field	34
4.2.4 Equations of Motion	36
4.2.5 Energy Considerations	37

	<u>Page</u>
4.3 Future Work	40
5. GENERAL CONCLUSIONS	40

LIST OF ILLUSTRATIONS

<u>Figure</u>		<u>Page</u>
3.1	Vector Plot of $T \times 10^{-2} / (P_{inb} / I_o V_o)$ for $d = 0$, $QC = 0.125$, $f_a / f_b = 1.1$, $C_b = 0.05$, $f_a C_a = f_b C_b$, $P_{ina} / I_o V_o = -43$ db.	5
3.2	Gain of the Output at f_a vs. Velocity Parameter b for $d = 0$, $QC = 0.125$, $f_a / f_b = 1.1$, $C_b = 0.05$, $f_a C_a = f_b C_b$, $P_{ina} / I_o V_o = -43$ db, $P_{inb} / I_o V_o = -53$ db.	7
3.3	Output Power at $2f_a - f_b$ Relative to the Output Power at f_a vs. Velocity Parameter b for $d = 0$, $f_a / f_b = 1.1$, $f_a C_a = f_b C_b$, $P_{ina} / I_o V_o = -43$ db, $P_{inb} / I_o V_o = -53$ db.	8
3.4	Amplitude Cross-Modulation Factor vs. Velocity Parameter b for $d = 0$, $f_a / f_b = 1.1$, $f_a C_a = f_b C_b$, $P_{ina} / I_o V_o = -43$ db, $\zeta = 5$.	10
3.5	Amplitude of the Complex Cross-Modulation Factor vs. Velocity Parameter b for $d = 0$, $f_a / f_b = 1.1$, $f_a C_a =$ $f_b C_b$, $P_{ina} / I_o V_o = -43$ db, $\zeta = 5$.	11
3.6	Phase of the Complex Cross-Modulation Factor vs. Velocity Parameter b for $d = 0$, $f_a / f_b = 1.1$, $f_a C_a =$ $f_b C_b$, $P_{ina} / I_o V_o = -43$ db, $\zeta = 5$.	12
3.7	Amplitude Cross-Modulation Factor vs. Frequency Ratio f_a / f_b for $d = b = QC = 0$, $C_b = 0.05$, $f_a C_a =$ $f_b C_b$, $P_{ina} / I_o V_o = -53$ db.	13
3.8	Output Power at $2f_a - f_b$ Relative to the Output Power at f_a vs. Total Input Power for $d = b = QC = 0$, $C_b = 0.05$, $f_a / f_b = 1.1$, $f_a C_a = f_b C_b$. The Input Power at f_b Is 10 db Higher than the Input at f_a . (The Dots Are Obtained Experimentally.)	14
3.9	Amplitude Cross-Modulation Factor vs. Frequency Ratio f_a / f_b for $d = b = QC = 0$, $C_b = 0.05$, $f_a C_a =$ $f_b C_b$, $P_{ina} / I_o V_o = -53$ db, $\zeta = 5$.	16

<u>Figure</u>		<u>Page</u>
3.10	Amplitude of the Complex Cross-Modulation Factor vs. Frequency Ratio f_a/f_b for $d = b = QC = 0$, $C_b = 0.05$, $f_a C_a = f_b C_b$, $P_{ina}/I_o V_o = -53$ db, $\zeta = 5$.	17
3.11	Phase of the Complex Cross-Modulation Factor vs. Frequency Ratio f_a/f_b for $d = b = QC = 0$, $C_b = 0.05$, $f_a C_a = f_b C_b$, $P_{ina}/I_o V_o = -53$ db, $\zeta = 5$.	18
3.12	Amplitude Cross-Modulation Factor vs. Velocity Parameter b for $d = QC = 0$, $f_a/f_b = 1.1$, $C_b = 0.05$, $f_a C_a = f_b C_b$, $P_{ina}/I_o V_o = -53$ db, $\zeta = 5$.	19
3.13	Experimental Measurement of Output Power vs. D-c Voltage for 3-Frequency Input Signals at $f_1 = 8.905$, $f_2 = 8.805$, $f_3 = 9.095$, $P_{inf_2} = P_{inf_3}$, P_{inf_1} Is 10 db Higher than P_{inf_2} , Total Input Power 3 dbm.	20
4.1	Normalized Axial Beam Velocity u/u_o vs. Normalized Beam Radius ρ .	26
4.2	Phase Slip vs. Normalized Beam Radius ρ with Pump Field Strength N as Parameter.	31
4.3	Pump Field Strength N vs. Maximum Normalized Beam Radius ρ_m .	32
4.4	Phase Slip vs. Normalized Beam Radius ρ with Initial Beam Radius ρ_o as Parameter Pump Field Strength $N = 0.05$.	33
4.5	Energy Relations vs. Normalized Beam Radius.	41

PERSONNEL

<u>Scientific and Engineering Personnel</u>		<u>Time Worked in</u> <u>Man Months*</u>
J. Rowe	Professors of Electrical Engineering	.45
C. Yeh		1.26
M. El-Shandwily	Research Associate	2.97
H. Detweiler	Assistant Research Engineers	.46
W. Rensel		.13
E. Fronczak	Research Assistants	.32
A. Heath		.55
B. Ho		1.41
R. Maire		.60
R. Ying		.18
<u>Service Personnel</u>		7.63

* Time Worked is based on 172 hours per month.

INTERIM SCIENTIFIC REPORT NO. 6

FOR

BASIC RESEARCH IN MICROWAVE DEVICES AND QUANTUM ELECTRONICS

1. General Introduction (C. Yeh)

The broad purpose of this project is to investigate new ideas in the area of microwave devices and quantum electronics. The program is envisioned as a general and flexible one under which a wide variety of topics may be studied. At present, the following areas of investigation are in progress:

A. Study of frequency multiplication in an angular propagating circuit. The design of the multiplier tube has been revised to enhance the overall efficiency. The parts for the new tube are presently being fabricated and assembly will be completed during the next period.

B. Investigation of high-thermal-conductivity materials for microwave devices above X-band. Work is continuing on the development of the BeO rod-metal envelope helix support structure. Upon completion of the structure, d-c heating tests and r-f cold tests will be conducted.

C. Analysis of amplitude- and phase-modulated traveling-wave amplifiers. Equations derived during various stages of the development using several methods of approach (i.e., the large-signal analysis, the analysis by the Boltzmann transport equation, etc.) will be programmed and computed. The theoretical results will then be compared with some experimental work.

D. Study of a d-c pumped quadrupole amplifier. Beam trajectories and energy relations will be studied in some detail. Equations for computing the trajectories applicable to the cyclotron-synchronous

mode of interaction will be derived and programmed for computation. Energy interchange between the axial and transverse velocities resulting in phase slip of the rotating beam with respect to the pumping field is discussed.

2. Generation and Amplification of Coherent Electromagnetic Energy in the Millimeter and Submillimeter Wavelength Region

2.1 Study of Frequency Multiplication in an Angular Propagating Circuit. (C. Yeh and B. Ho)

The fabrication of the tube parts has been unexpectedly delayed due to tooling problems. To date the multipole-cavity portion of the multiplier has been completed. After the coupling loop has been attached, the cavity will undergo a cold test to determine its resonant frequency and the extent of moding problems. After that the coupling loop will be adjusted to achieve a maximum coupling and the best impedance matching. Assembly and processing of the remainder of the tube will follow.

2.2 Investigation of High-Thermal-Conductivity Materials for Devices Above X-Band. (H. K. Detweiler)

2.2.1 Introduction. Work on developing the BeO rod-metal tube structure was continued during this period. Further attempts have been made to find a technique for deforming the metal envelope to permit insertion of the helix-BeO rod assembly. Also tests have been conducted on brazing ceramic rods to a tungsten helix. A detailed account of the work is given below.

2.2.2 Experimental Effort. During the previous quarter it was determined that the copper tubing to be used in the BeO rod-metal envelope structure could not be elastically deformed more than approximately one mil for the insertion of the brazed BeO rod-helix assembly.

Since it was felt that this would not be sufficient clearance for loading the helix assembly, stainless steel tubing was obtained. During this period, tests were conducted on this tubing to determine if it could be elastically deformed more than the copper tubing. After several unsuccessful tries it was concluded that the jig used was not strong enough for the stainless steel tubing. Since it will require another jig to evaluate this tubing, it has been decided to postpone this step until it has been determined whether it is possible to assemble the structure using the copper tubing.

Some progress has been made on brazing ceramic rods to the tungsten helix. Early in the period a cold-rolled-steel jig was made for holding the rods in contact with the helix during brazing. A brazing test was conducted using this jig with a 0.030 inch tungsten helix and three 0.030 inch diameter sapphire rods. Brazing did take place; however, the ceramic rods were quite dirty due to evaporating materials coming out of the steel jig. A new jig was made out of stainless steel and further brazing tests were then conducted. The first test was unsuccessful due to an insufficient amount of titanium on the helix. The second test, with more titanium present, was successful. In this test three 0.030 inch diameter BeO rods were brazed to a tungsten helix having 64 TPI, a 5 mil wire diameter and being 4-7/8 inches long. The plating thicknesses were 0.102 mil of copper and 0.11 mil of titanium. The assembly was vacuum fired at 1030°C for 1-1/2 minutes. Attempts will be made during the next period to load this assembly into a copper tube and then heat test the structure.

2.2.3 Future Work. Work will continue on the development of the BeO rod-metal envelope helix support structure. This structure will be heat tested upon its successful fabrication.

3. Analysis of Amplitude- and Phase-Modulated Traveling-Wave Amplifiers

(M. E. El-Shandwily and J. E. Rowe)

3.1 Introduction. In the previous progress report (No. 5) there were noted four items for future study. These are as follows:

1. Obtaining additional results for the analysis presented in Quarterly Progress Report No. 1 (integration of equations of motion method).
2. Obtaining computer results for the analysis presented in Quarterly Progress Report No. 3 (Boltzmann transport equation method).
3. Continuing the experimental work to study the operation of the TWA with three or four input signals.
4. Detecting and correcting the error in the computer program of the large-signal analysis (Quarterly Progress Report No. 4).

The work accomplished during this period on each of the above items will be reported in the following section.

3.2 Results.

3.2.1 Theoretical Results from the Integration of Equations of Motion Method. Numerical results have been obtained for many interesting values of the traveling-wave amplifier parameters with two input signals. Some of the results obtained are presented in the form of graphs throughout this section.

Figure 3.1 is a vector plot of the complex cross-modulation factor T . The solid curves show the variation of the complex cross-modulation factor at constant normalized distance, $\zeta(\beta_e C z)$, for a variable velocity parameter, b . The dotted curves show the variation of T at constant b for variable ζ . Any point in the complex plane gives the real and imaginary parts (or amplitude and phase) of T for a particular b and ζ .

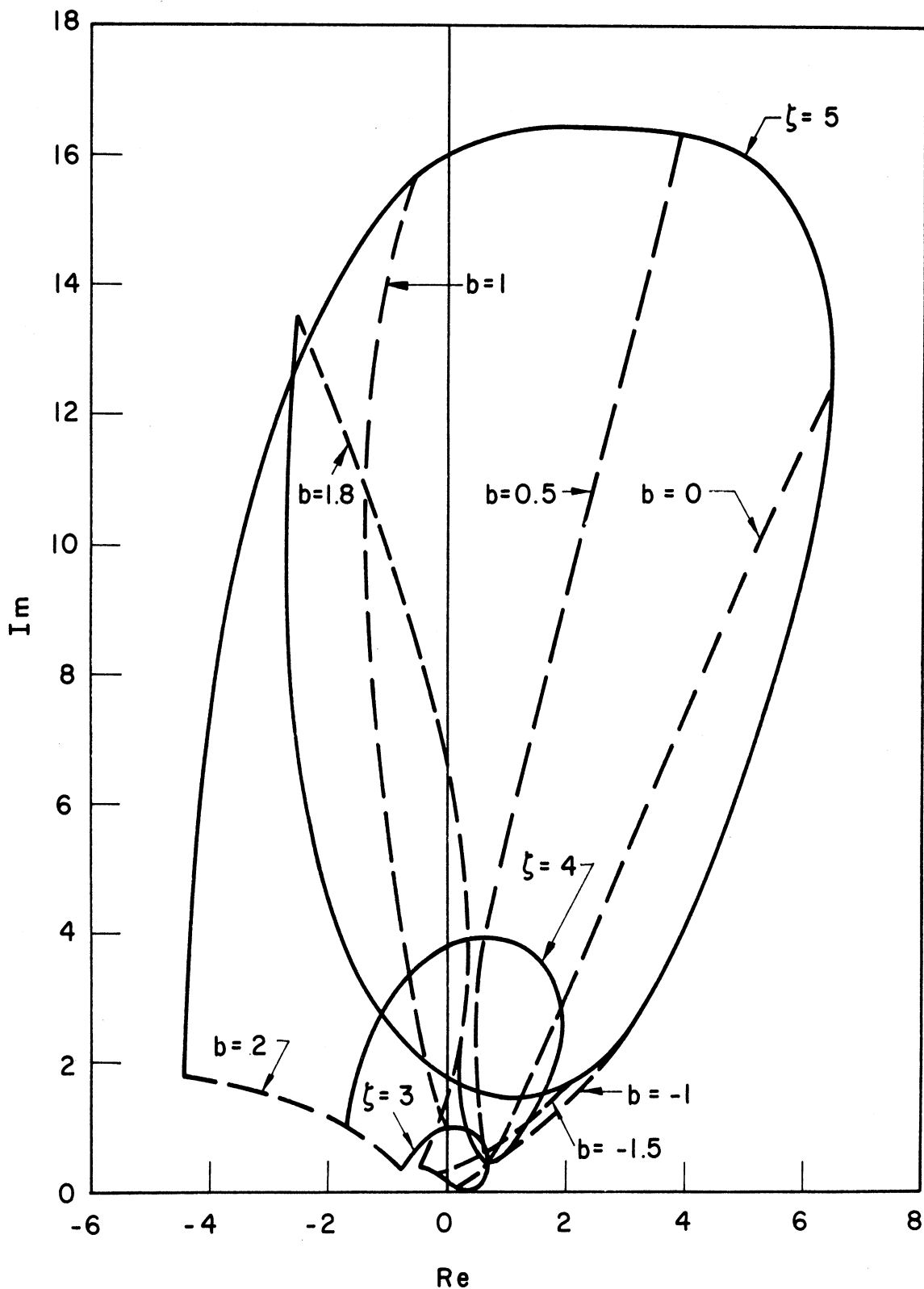


FIG. 3.1 VECTOR PLOT OF $T_x 10^{-2} / (P_{inb} / I_o V_o)$ FOR $d = 0$, $QC = 0.125$,
 $f_a / f_b = 1.1$, $C_b = 0.05$, $f_a C_a = f_b C_b$, $P_{ina} / I_o V_o = -43$ db.

This equation is useful because it defines the quantities which must be measured in the experiment. These are Q , the heat added to the calorimeter, F , the flow rate through the calorimeter, T , the temperature rise through the calorimeter, $-\left(\frac{\partial H}{\partial P}\right)_{T_x} \frac{\partial P}{\Delta T}$ the correction to the mean heat capacity due to the pressure drop through the calorimeter, and $\frac{\delta Q}{F\Delta T}$ the correction due to heat leakage. This equation also gives an indication of what is desirable in a properly designed calorimeter. The design should include provisions for accurately measuring the heat added to the calorimeter, the flow through it, and the temperature rise of the fluid. In addition it is desirable to have the pressure drop and the heat losses as small as possible to minimize these corrections to the principle measurement.

The design, construction and operation of the equipment has been discussed in detail by Faulkner¹² and Jones¹⁵. A schematic diagram of the flow system used in this investigation is shown in Figure 1. The principle elements of the system are the compressor used to circulate the gas, cooling baths used to bring the gas to the desired initial temperature, the flow calorimeter, valves to throttle the gas to lower pressure, the flow metering apparatus, and the storage tanks.

This equipment had been used previously to make enthalpy determinations on pure components. When the study of the methane-propane system was undertaken, early experiments indicated that many major modifications to the equipment were necessary in order to make it suitable for use with

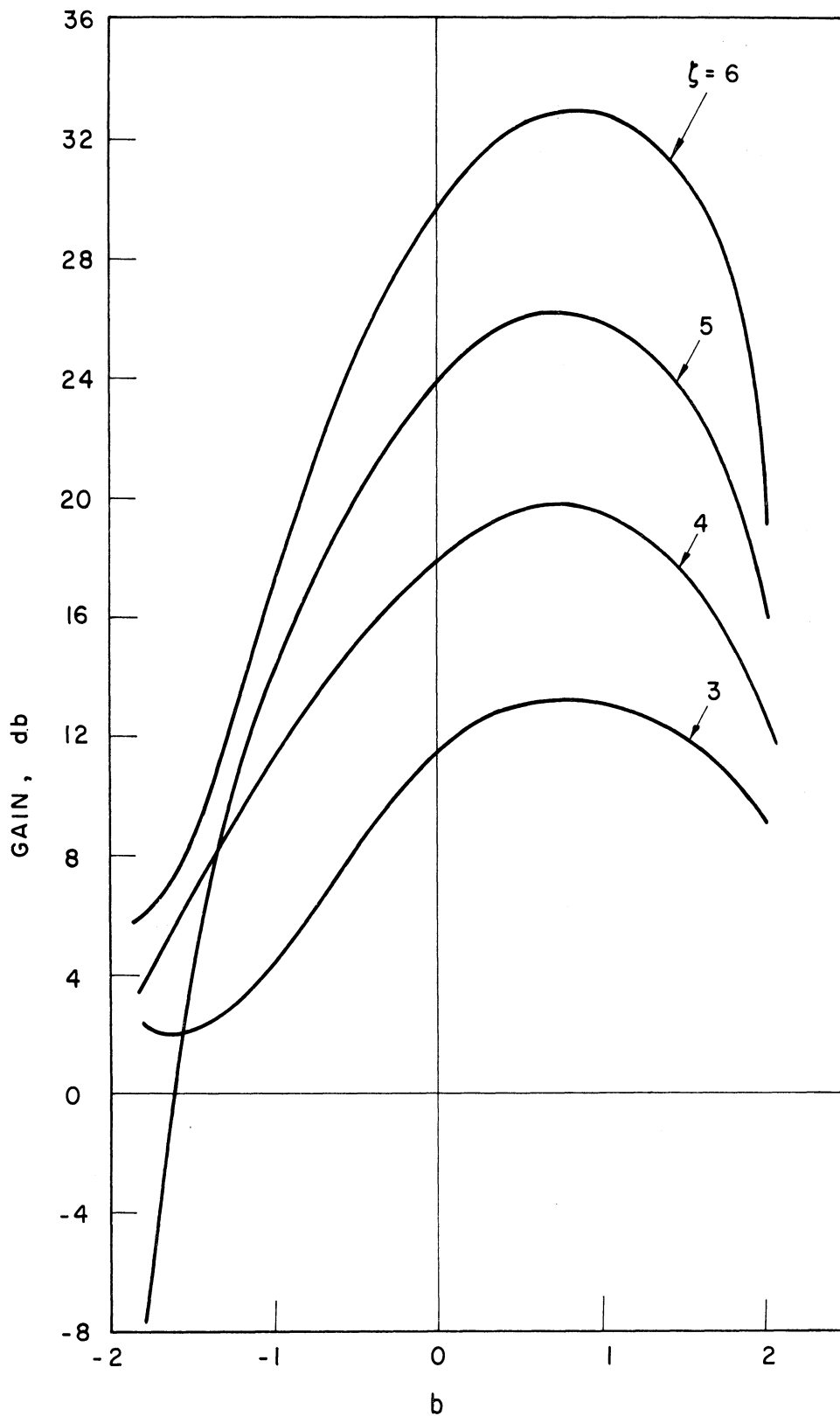


FIG. 3.2 GAIN OF THE OUTPUT AT f_a VS. VELOCITY PARAMETER b FOR $d = 0$,
 $QC = 0.125$, $f_a/f_b = 1.1$, $C_b = 0.05$, $f_a C_a = f_b C_b$, $P_{ina}/I_o V_o =$
 -43 db, $P_{inb}/I_o V_o = -53$ db.

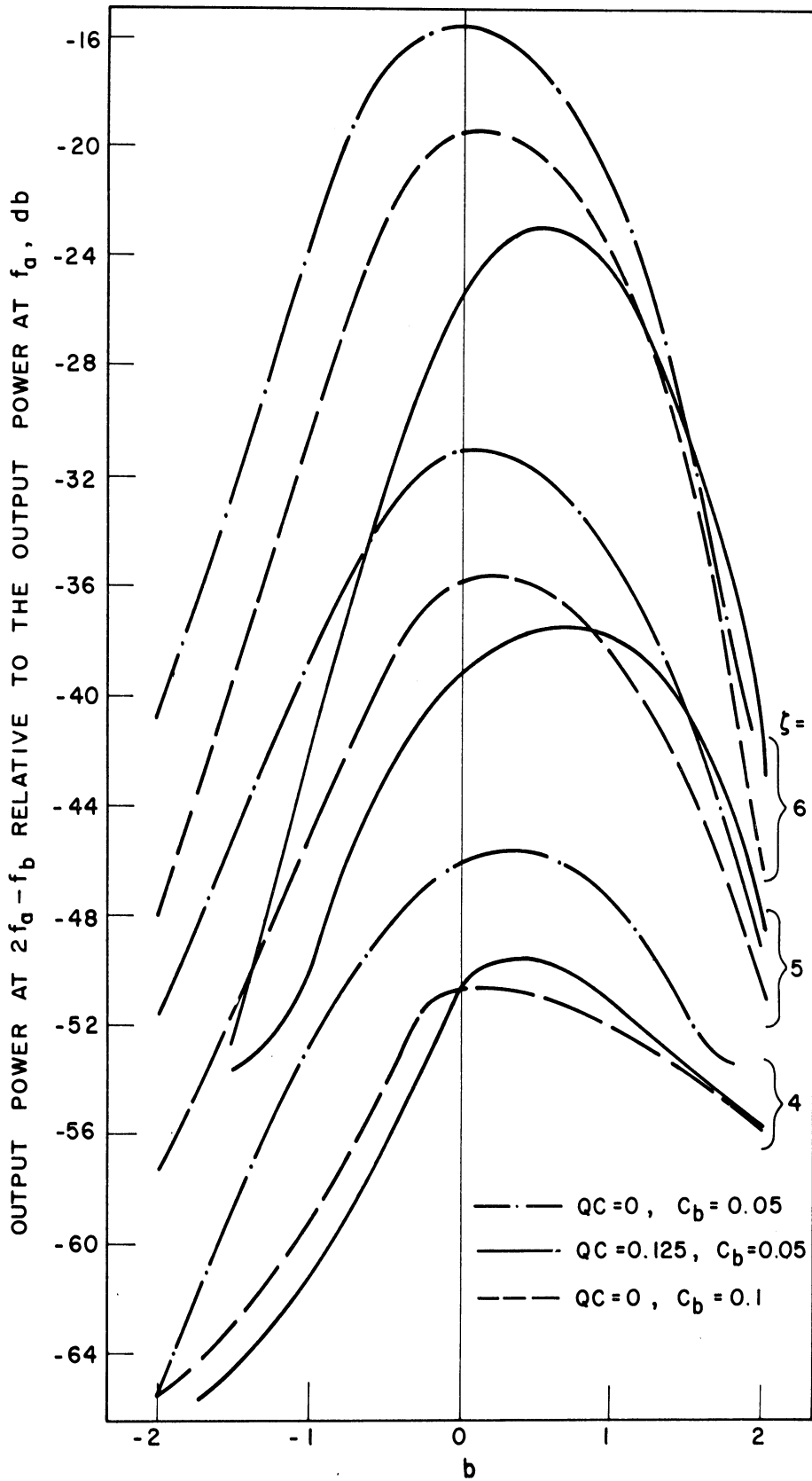


FIG. 3.3 OUTPUT POWER AT $2f_a - f_b$ RELATIVE TO THE OUTPUT POWER AT f_a VS. VELOCITY PARAMETER b FOR $d = 0$, $f_a/f_b = 1.1$, $f_a C_a = f_b C_b$, $P_{ina}/I_o V_o = -43$ db, $P_{inb}/I_o V_o = -53$ db.

Figure 3.4 is a plot of the amplitude cross-modulation factor T' vs. b for $\xi = 5$. The amplitude cross-modulation factor T' is defined as

$$T' = 1 - \left| \frac{P_{\text{out } f_1} \text{ when } P_{\text{in } f_2} \neq 0}{P_{\text{out } f_1} \text{ when } P_{\text{in } f_2} = 0} \right|^{1/2}$$

It is seen from these figures that in all cases considered T' goes to zero for values of b close to 1. When T' is zero there will be no change in the output power at f_a due to the presence of another signal at f_b . It is seen from the figures that the presence of space-charge forces or the increase of the value of C reduces the value of T' .

Figure 3.5, is a plot of the amplitude of the complex cross-modulation factor vs. b for $\xi = 5$. Again one observes that the presence of space-charge forces reduces the amplitude of the complex cross-modulation factor.

Figure 3.6 shows the variation of the phase of the complex cross-modulation factor with b for $\xi = 5$. It is seen that for $QC = 0$, $C_b = 0.05$ and $QC = 0$, $C_b = 0.1$, the phase goes to zero for values of b between -1 and -1.5. When the phase of T is zero T will be real and there will be no change in the phase of the output signal at f_a due to the presence of the signal at f_b .

The change of the amplitude cross modulation with the frequency ratio f_a/f_b is shown in Fig. 3.7. It is seen from this figure that T' increases with the increase of f_a/f_b . This indicates that the change in the output power at f_a due to the presence of the other signal at f_b is small when the ratio f_a/f_b is small.

Figure 3.8 shows the variation of the output power at $2f_a - f_b$ relative to the output power at f_a with the total input power for various

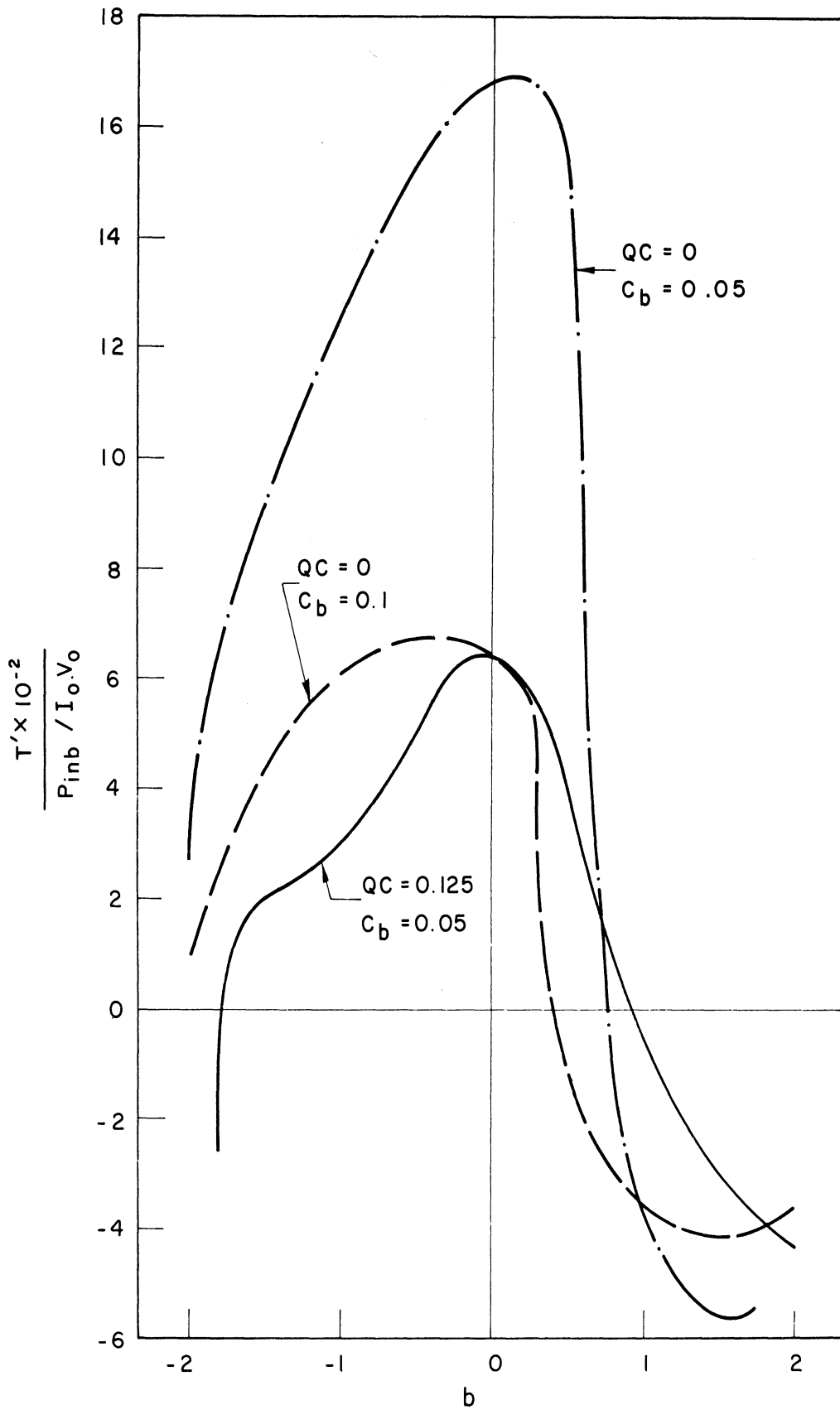


FIG. 3.4 AMPLITUDE CROSS-MODULATION FACTOR VS. VELOCITY PARAMETER b

FOR $d = 0$, $f_a/f_b = 1.1$, $f_a C_a = f_b C_b$, $P_{ina}/I_0 V_0 = -43$ db, $\zeta = 5$.

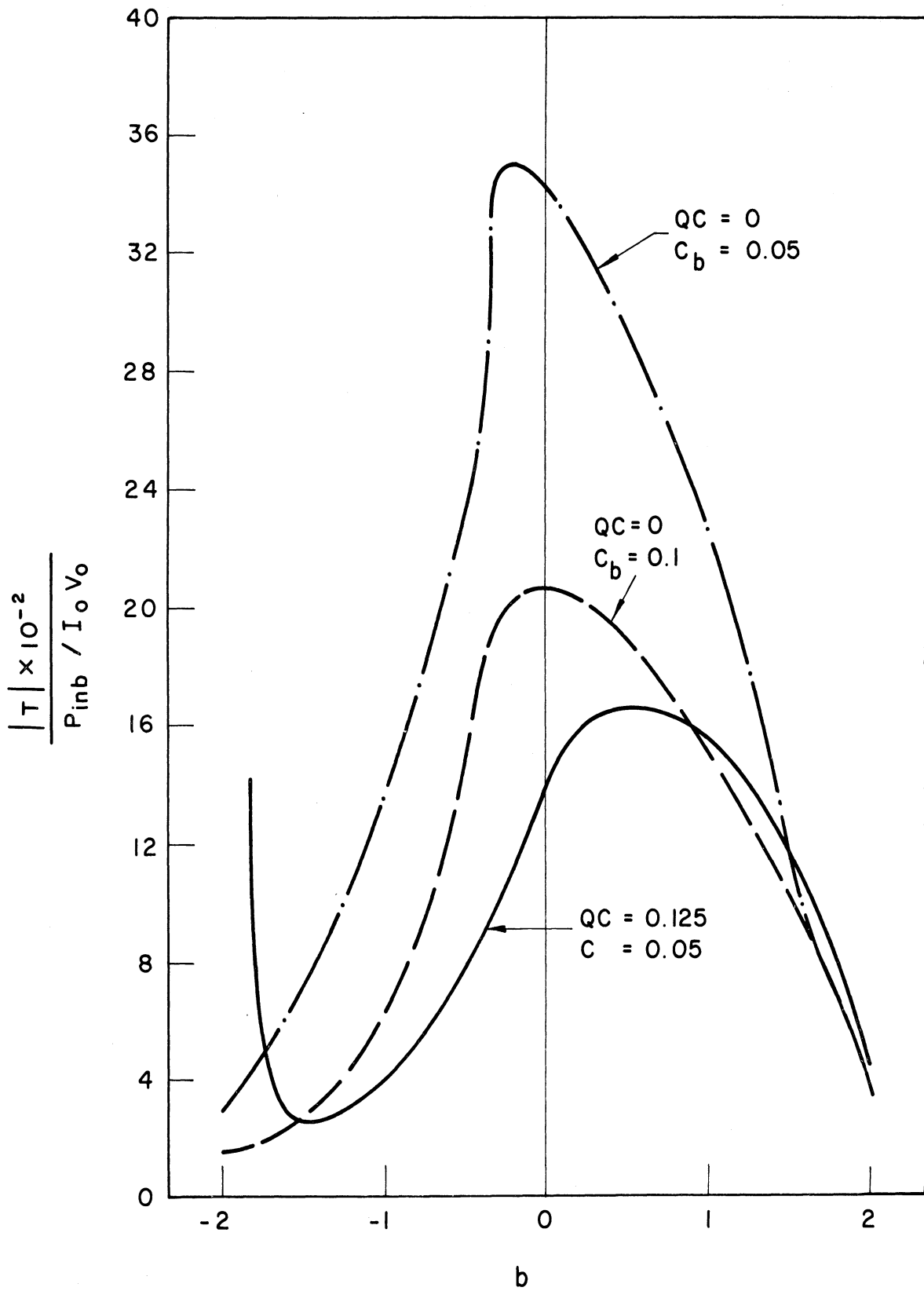


FIG. 3.5 AMPLITUDE OF THE COMPLEX CROSS-MODULATION FACTOR VS. VELOCITY
PARAMETER b FOR $d = 0$, $f_a/f_b = 1.1$, $f_a C_a = f_b C_b$, $P_{ina}/I_0 V_0 =$
 -43 db, $\zeta = 5$.

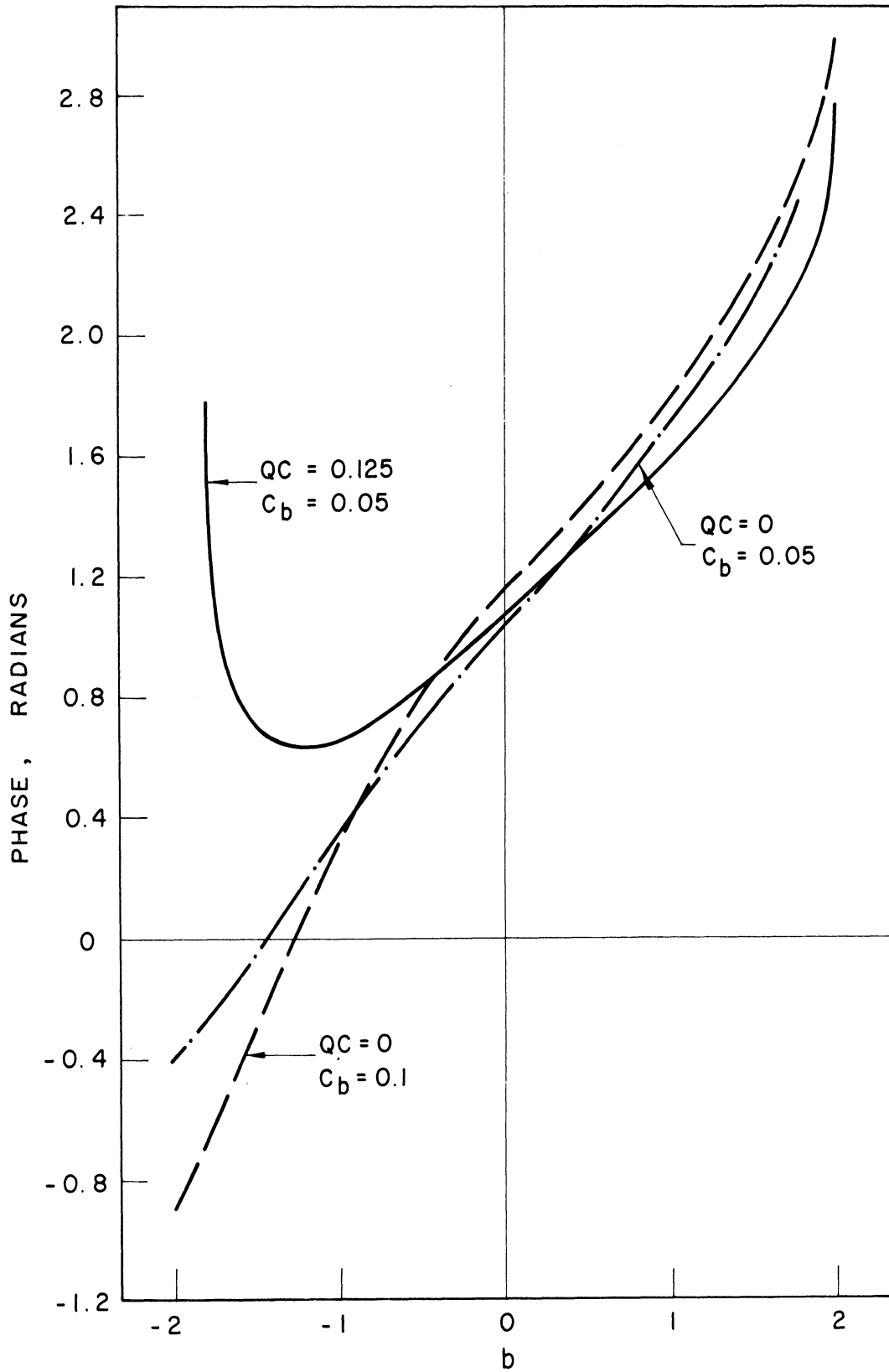


FIG. 3.6 PHASE OF THE COMPLEX CROSS-MODULATION FACTOR VS. VELOCITY PARAMETER b FOR $d = 0$, $f_a/f_b = 1.1$, $f_a C_a = f_b C_b$, $P_{ina}/I V_{oo} = -43$ db, $\zeta = 5$.

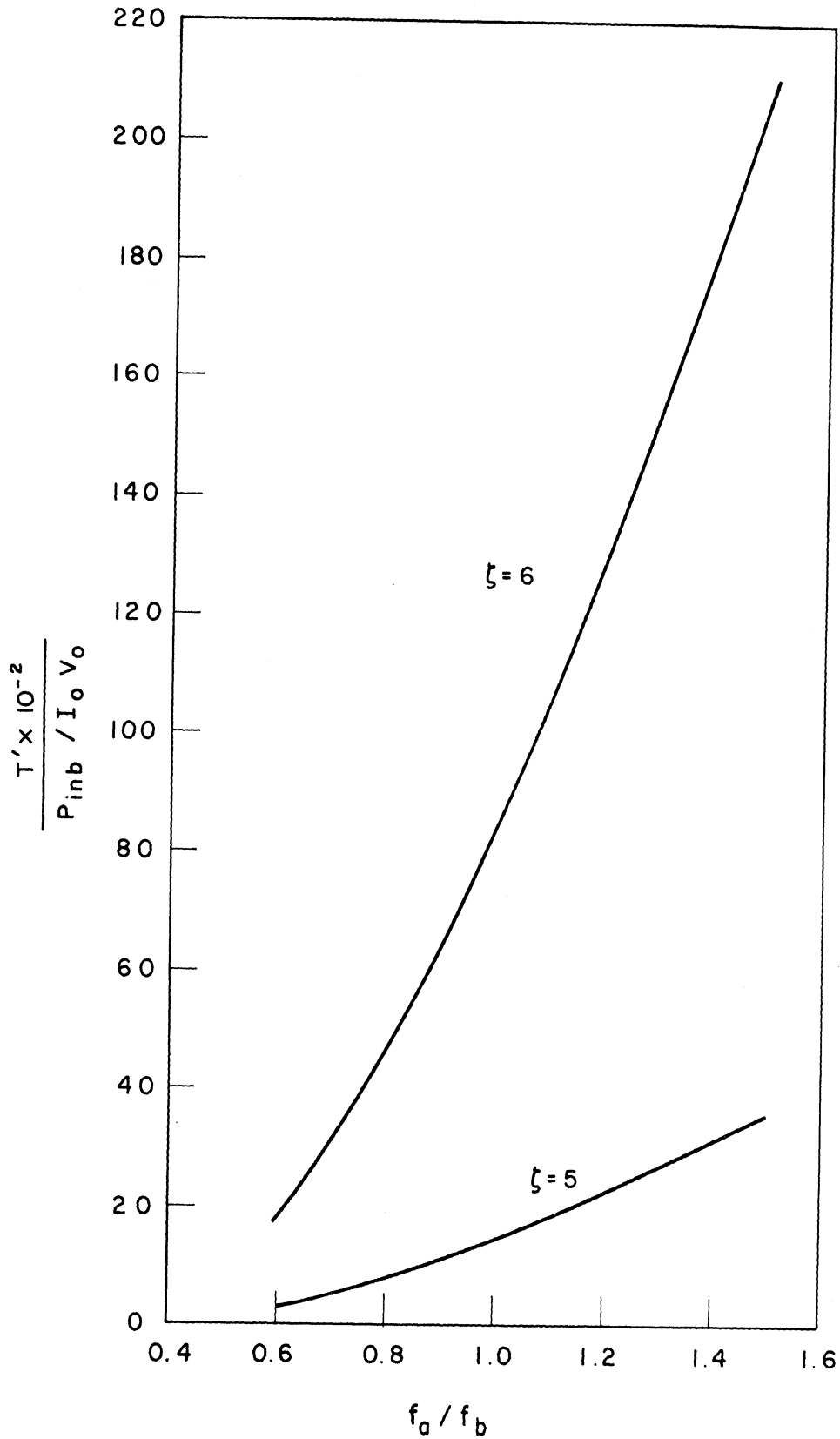


FIG. 3.7 AMPLITUDE CROSS-MODULATION FACTOR VS. FREQUENCY RATIO f_a / f_b

FOR $d = b = QC = 0$, $C_b = 0.05$, $f_a C_a = f_b C_b$, $P_{ina} / I_0 V_0 = -53$ db.

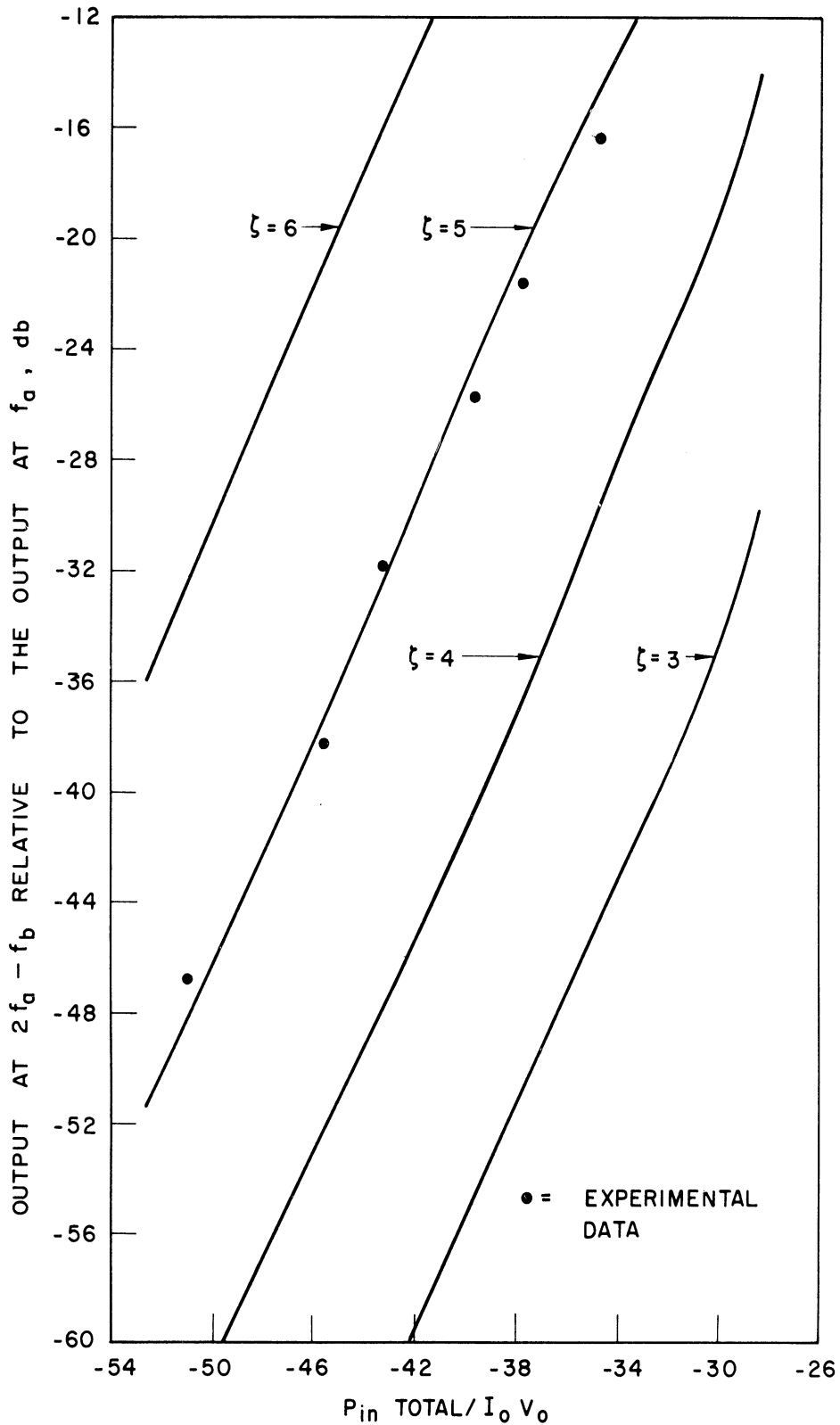


FIG. 3.8 OUTPUT POWER AT $2f_a - f_b$ RELATIVE TO THE OUTPUT POWER AT f_a VS. TOTAL INPUT POWER FOR $d = b = QC = 0$, $C_b = 0.05$, $f_a/f_b = 1.1$, $f_a C_a = f_b C_b$. THE INPUT POWER AT f_b IS 10 db HIGHER THAN THE INPUT AT f_a . (THE DOTS ARE OBTAINED EXPERIMENTALLY.)

values of ζ . The points shown around the line $\zeta = 5$ are obtained experimentally. The theoretical curves are obtained for the case where $QC = 0$, $C_b = 0.05$, $d = 0$ and $b = 0$. The experimental points are obtained with the d-c voltage adjusted for maximum small-signal gain, but the space-charge forces and the loss must have some finite values. However, the comparison indicates the same type of variation between the theoretical and experimental results.

3.2.2 Boltzmann Transport Equation Method. The analysis of the TWA with two input signals using the Boltzmann transport equation was presented in Quarterly Progress Report No. 3. The equations have been solved on a digital computer. Some of the results are shown in the form of graphs in Figs. 3.9 through 3.12. The results obtained from the integration of the equations of motion method (Quarterly Progress Report No. 1) are also shown for comparison. The most striking difference between the two methods appears in Fig. 3.11 for the phase of T vs. the frequency ratio. It should be noted that in the Boltzmann transport equation method only the growing wave for each input signal was considered. In the integration of the equations of motion method all three waves for each input signal were considered.

Figures 3.9, 3.10 and 3.11 are plots of T' , $|T|$ and phase of T vs. the frequency ratio f_a/f_b respectively. The shape of the curves is the same except for a difference in magnitude.

Figure 3.12, is a plot of T' vs. b for $\zeta = 5$. Again the results from the two methods have the same kind of variation but there is a difference in magnitude.

3.2.3 Experimental Work. Some results of the measurements made on an X-band, medium power, traveling-wave amplifier with three input signals are shown in Fig. 3.13. It is to be noted that with three

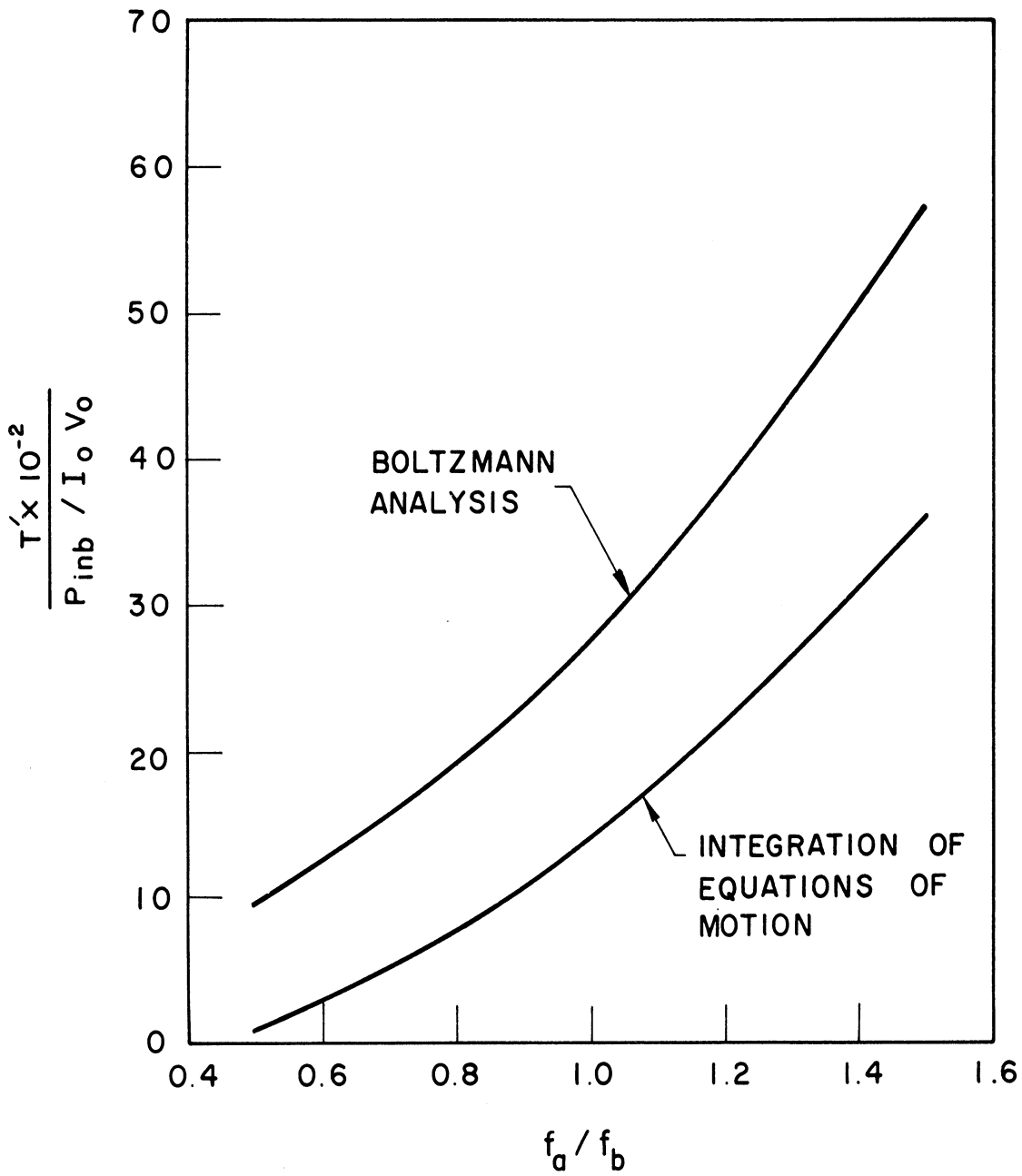


FIG. 3.9 AMPLITUDE CROSS-MODULATION FACTOR VS. FREQUENCY RATIO f_a/f_b
 FOR $d = b = QC = 0$, $C_b = 0.05$, $f_a C_a = f_b C_b$, $P_{ina} / I_o V_o = -53$ db,
 $\zeta = 5$.

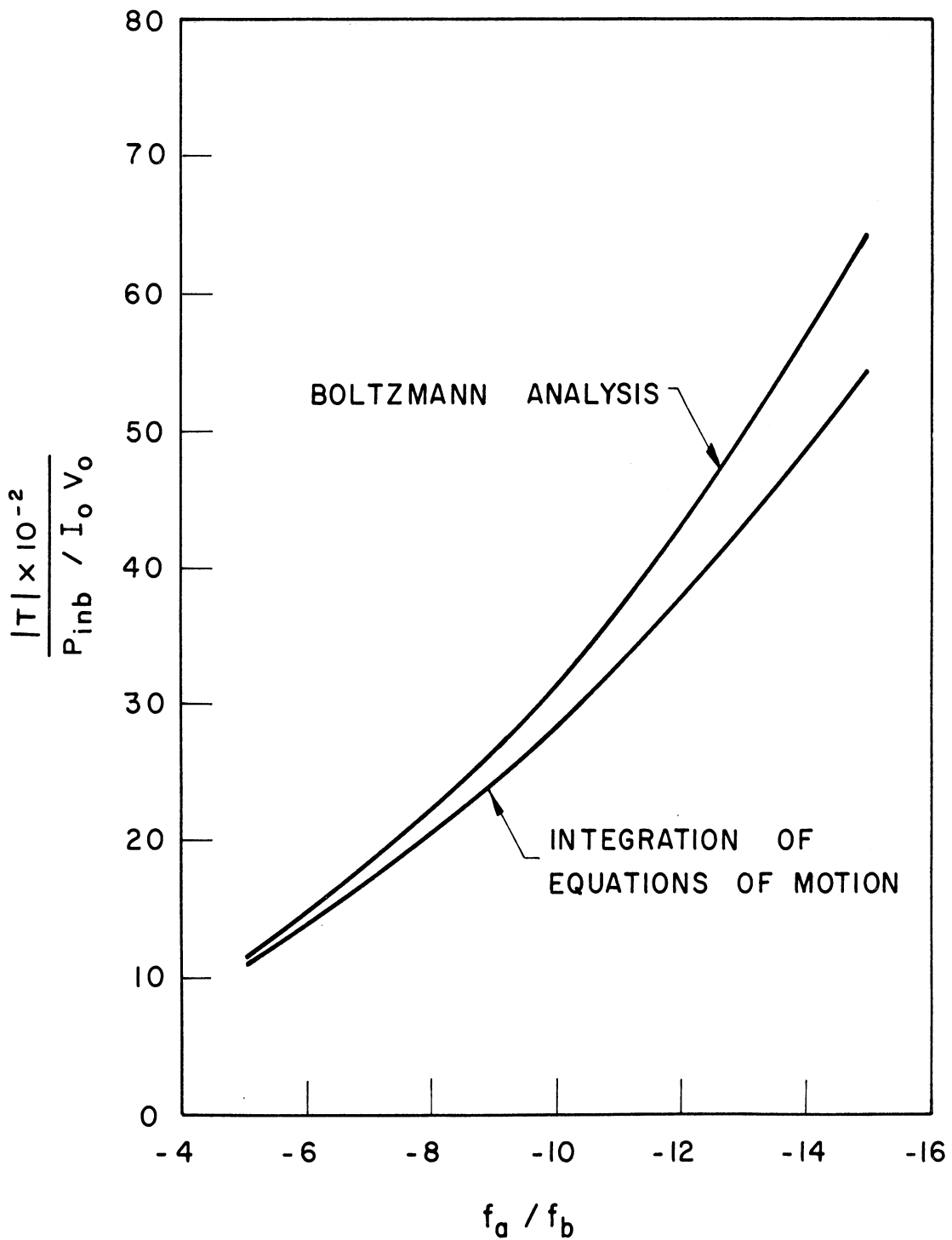


FIG. 3.10 AMPLITUDE OF THE COMPLEX CROSS-MODULATION FACTOR VS. FREQUENCY

RATIO f_a / f_b FOR $d = b = QC = 0$, $C_b = 0.05$, $f_a C_a = f_b C_b$,

$P_{ina} / I_0 V_0 = -53$ db, $\zeta = 5$.

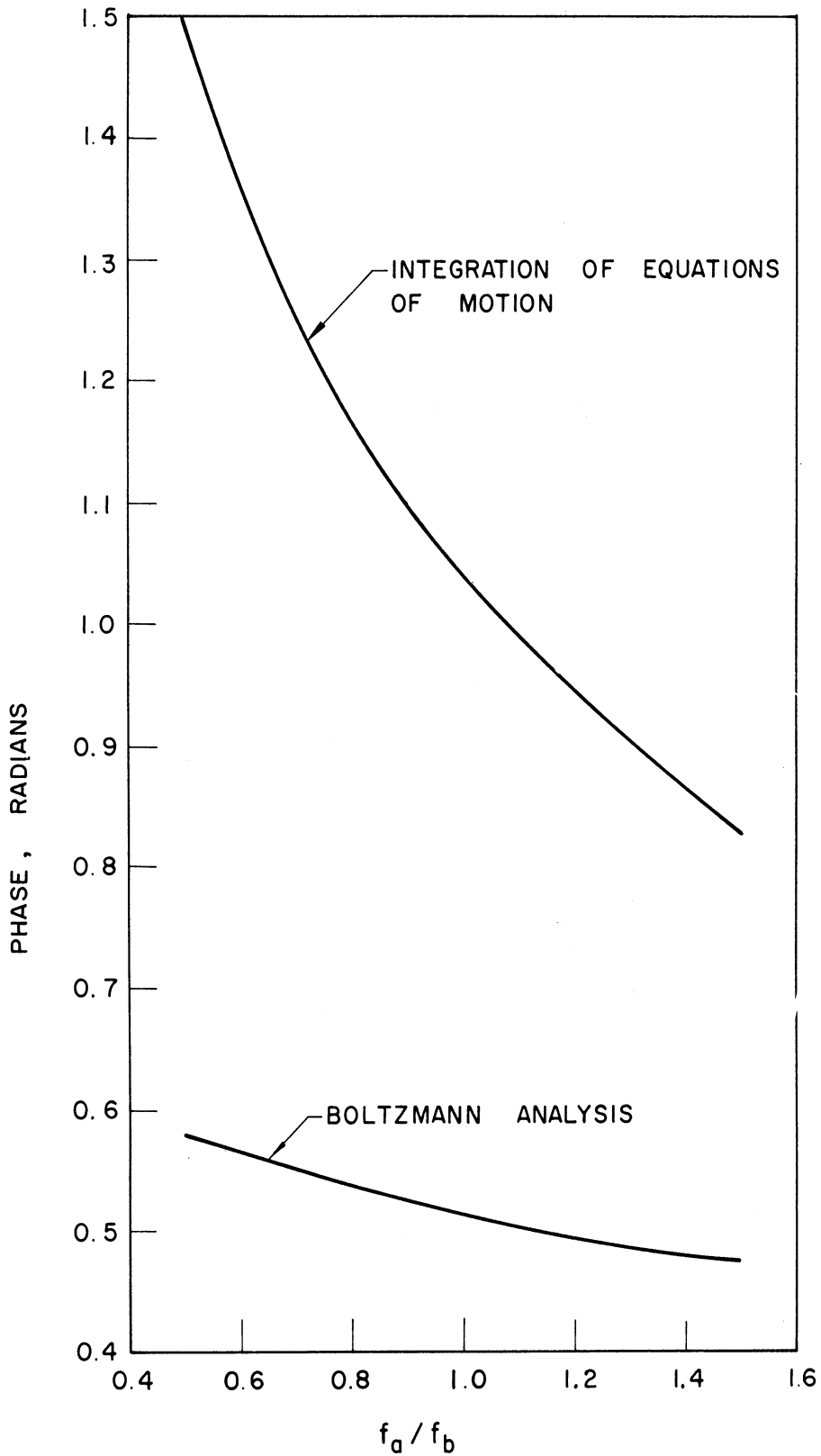


FIG. 3.11 PHASE OF THE COMPLEX CROSS-MODULATION FACTOR VS. FREQUENCY

RATIO f_a/f_b FOR $d = b = QC = 0$, $C_b = 0.05$, $f_a C_a = f_b C_b$,

$P_{ina}/I_o V_o = -53$ db, $\zeta = 5$.

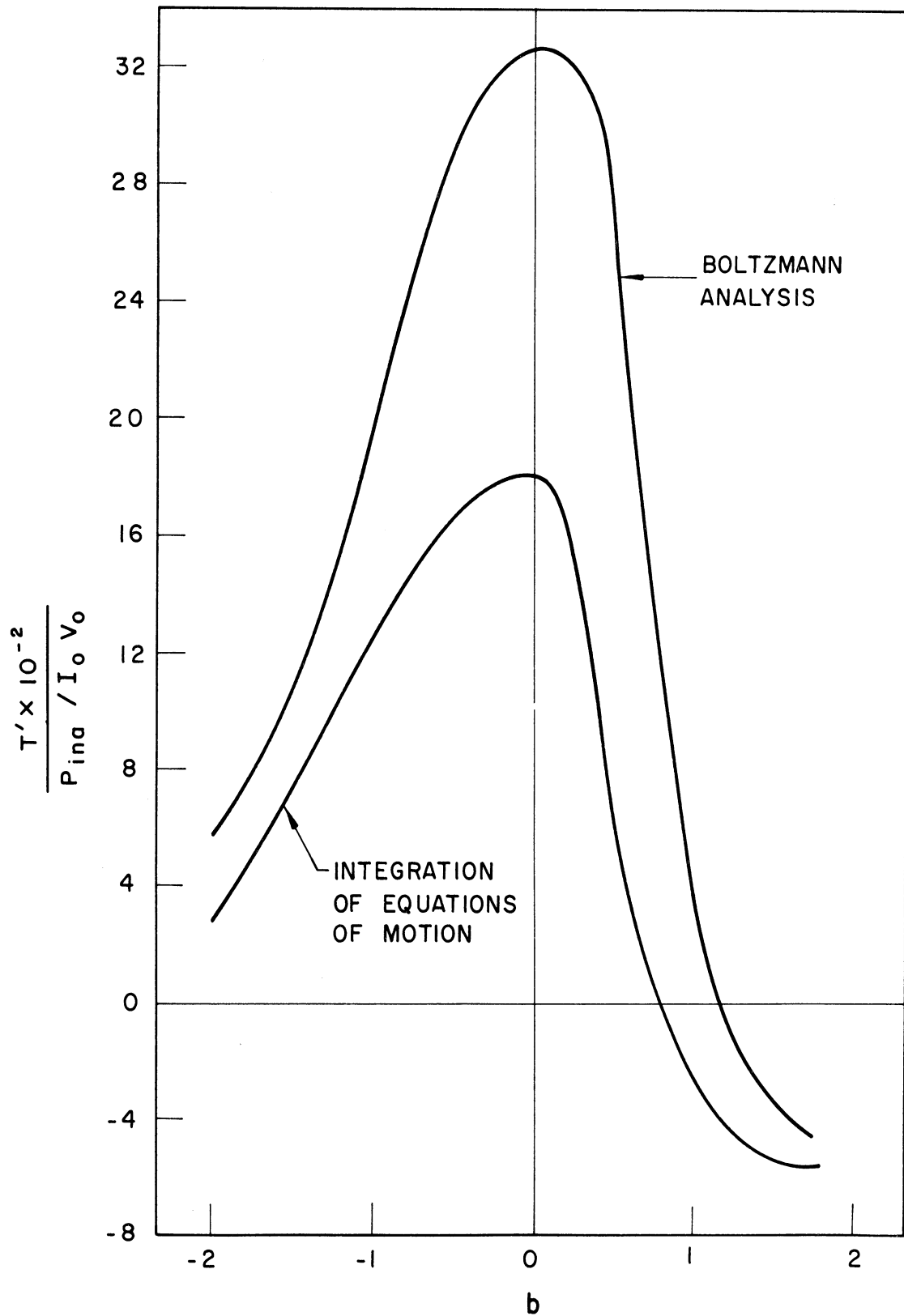


FIG. 3.12 AMPLITUDE CROSS-MODULATION FACTOR VS. VELOCITY PARAMETER b

FOR $d = QC = 0$, $f_a/f_b = 1.1$, $C_b = 0.05$, $f_a C_a = f_b C_b$, $P_{ina}/I_0 V_0 =$

- 53 db, $\zeta = 5$.

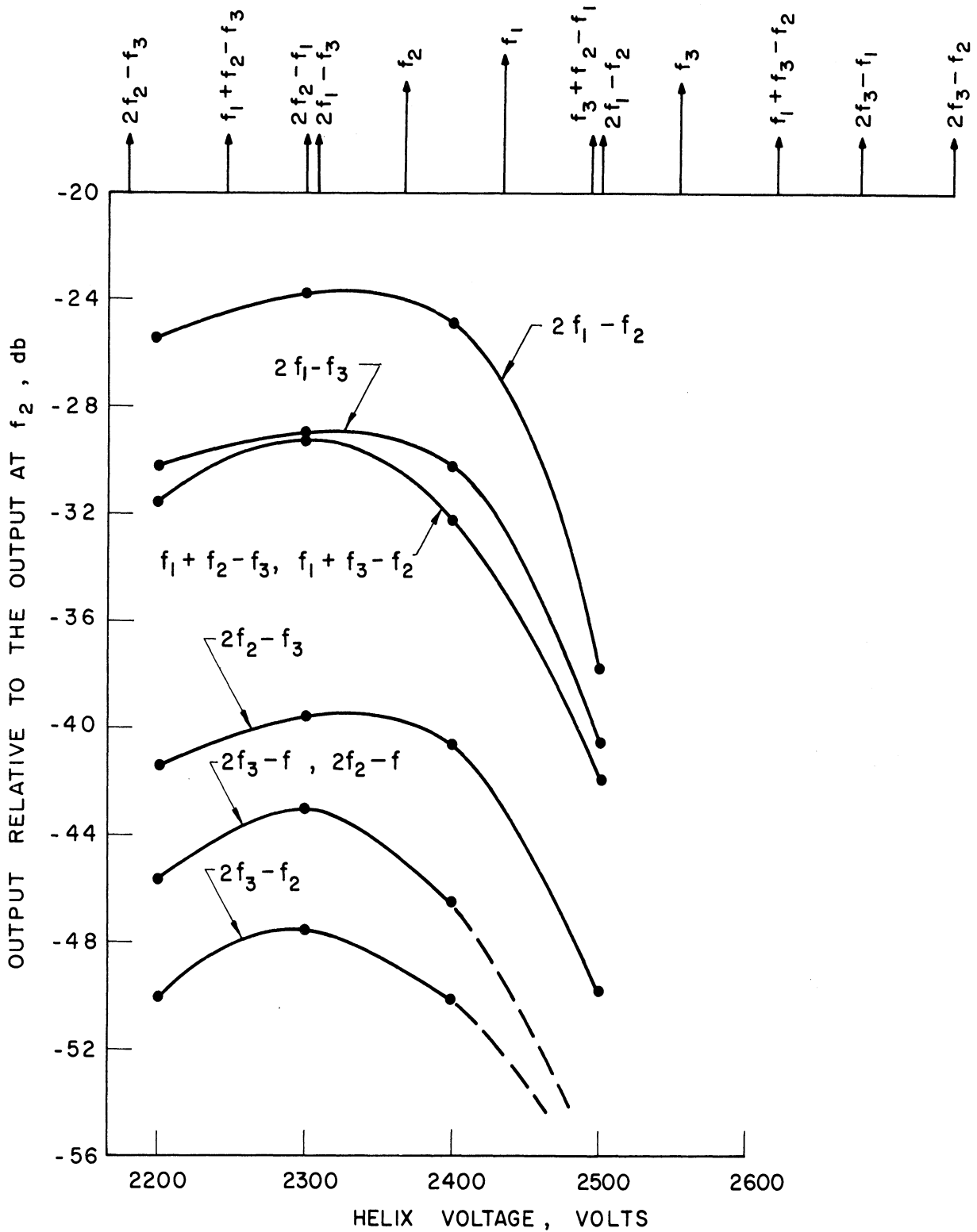


FIG. 3.13 EXPERIMENTAL MEASUREMENT OF OUTPUT POWER VS. D-C VOLTAGE FOR 3-FREQUENCY INPUT SIGNALS AT $f_1 = 8.905$, $f_2 = 8.805$, $f_3 = 9.095$, $P_{inf_2} = P_{inf_3}$, P_{inf_1} IS 10 db HIGHER THAN P_{inf_2} , TOTAL INPUT POWER 3 dbm.

input signals, assuming no harmonic propagation, there will be nine generated signals in the passband of the circuit. This can be seen from the following simple analysis. Assume the output-input characteristic can be written as

$$V_{\text{out}} = a_1 V_{\text{in}} + a_3 V_{\text{in}}^3 \quad (2.1)$$

Assume the input as

$$V_{\text{in}} = b_1 \cos \omega_1 t + b_2 \cos \omega_2 t + b_3 \cos \omega_3 t \quad (2.2)$$

Substitute Eq. 2 into Eq. 1 to obtain

$$V_{\text{out}} = a_1 (b_1 \cos \omega_1 t + b_2 \cos \omega_2 t + b_3 \cos \omega_3 t) + a_3 (b_1 \cos \omega_1 t + b_2 \cos \omega_2 t + b_3 \cos \omega_3 t)^3 \quad (2.3)$$

Expand the cubic term and reduce each term in the resulting expansion to the type $\cos (n_1 \omega_1 + n_2 \omega_2 + n_3 \omega_3) t$ so that the output can be written as

$$\begin{aligned} V_{\text{out}} = & [a_1 b_1 + a_3 (3/4 b_1^3 + 3/2 b_1 b_2^2 + 3/2 b_1 b_3^2)] \cos \omega_1 t \\ & + [a_1 b_2 + a_3 (3/4 b_2^3 + 3/2 b_2 b_1^2 + 3/2 b_2 b_3^2)] \cos \omega_2 t \\ & + [a_1 b_3 + a_3 (3/4 b_3^3 + 3/2 b_3 b_1^2 + 3/2 b_3 b_2^2)] \cos \omega_3 t \\ & + 3/4 b_1 b_2^2 \cos (2\omega_2 - \omega_1) t + 3/4 b_1 b_3^2 \cos (2\omega_3 - \omega_1) t \\ & + 3/4 b_3^2 b_2 \cos (2\omega_3 - \omega_2) t + 3/4 b_1^2 b_2 \cos (2\omega_1 - \omega_2) t \\ & + 3/4 b_1^2 b_3 \cos (2\omega_1 - \omega_3) t + 3/4 b_2^2 b_3 (\cos 2\omega_2 - \omega_3) t \\ & + 3/4 b_1 b_2 b_3 \cos (\omega_1 + \omega_2 - \omega_3) t + 3/4 b_1 b_2 b_3 \cos (\omega_1 + \omega_3 - \omega_2) t \\ & + 3/4 b_1 b_2 b_3 \cos (\omega_2 + \omega_3 - \omega_1) t + \dots \end{aligned}$$

Figure 3.13 shows the variation of the measured relative output power of each of the nine generated components with the d-c voltage. The variation is similar to that for the two input-signal case.

3.2.4 Large-Signal Analysis. In Quarterly Progress Report No. 4 a large-signal analysis for the multi-signal operation of the TWA was reported. Some numerical results were presented in the form of figures. It is believed that those figures are not correct due to an error in the computer program. This error has been detected and corrected. In addition it was found that the accuracy of the IBM 7090 digital computer is not sufficient to obtain correct results. This is due to the fact that the amplitude of a generated component at a particular frequency is calculated from the component of the beam charge density at that frequency. The components of the beam charge density are given as integrals of the form

$$\int_0^{2\pi L} \frac{\cos (n_1 \phi_1 + \dots + n_N \phi_N)}{1+2C_1 u} d\phi_{01}$$

and

$$\int_0^{2\pi L} \frac{\sin (n_1 \phi_1 + \dots + n_N \phi_N)}{1+2C_1 u} d\phi_{01} .$$

At the input where the phases of the entering electrons with respect to one of the input signals are equally spaced these integrals should be zero. Due to the limited accuracy of the computer, these integrals have finite values. These finite values will not affect the input signals since the integrals will be added to the input amplitudes which are relatively much larger. However, since the generated components start from zero, their amplitudes at a very short distance from the input are

proportional to these integrals. It could happen that the amplitude of one of the generated components starts with a negative value due to inaccuracy of the calculation of the charge density component and thus it will continue to grow negatively. This is due to the nature of the equations.

It is seen from the above that the accuracy of the computation has to be very high in order to obtain correct results. The computer program is being rewritten using a double precision method to achieve this accuracy.

3.3 Future Work. Work will continue on the large-signal analysis. The analysis is not limited to any signal level or any number of signals. It should give good results in and beyond the saturation region. Also it is planned to write a separate report covering all the findings for the multi-signal operation of the traveling-wave amplifiers.

4. Study of a D-c Pumped Quadrupole Amplifier (C. Yeh and B. Ho)

4.1 Introduction. In a previous progress report (No. 3), a coupled-mode theory was used to study the coupling between the cyclotron and synchronous waves in a quadrifilar type d-c pumped quadrupole amplifier. An anomalous gain was predicted above a certain pumping level. In Quarterly Progress Report No. 4 the kinetic power theorem was used to explain the power relations between various waves involved in the interaction. Since the high gain occurs under a strong pump field condition, the small-signal theory would not be adequate to describe the actual interaction, and a large-signal theory should be used to analyze the electron behavior during the entire amplifying process. The exact solution for the electron trajectories will be obtained with the aid of electronic computers.

4.2 Large-Signal Analysis of Quadrifilar D-c Pump Cyclotron-Synchronous Wave Quadrupole Amplifier.

4.2.1 Assumptions for the Analysis. The exact behavior of the individual electron in the pump field region of a quadrifilar d-c pumped quadrupole amplifier is extremely complex. The following assumptions are made to simplify the analysis:

1. Space-charge effects are neglected.
2. A filamentary electron beam is assumed, and beam expansion is neglected.
3. The axial magnetic field is constant, which implies that the beam is rotating at a constant angular velocity ω_c .
4. The pump field is not affected by the presence of the beam.

4.2.2 The Axial Beam Velocity and Phase Slip. In a small-signal analysis one assumes a constant axial beam velocity and the phase of the electrons with respect to the pump field is the same as they travel along the beam axis. These assumptions are true for the operation with a small beam radius. However, when the amplification of the device is large, the electrons behave quite differently from the above situation. Because of the amplification of the beam radius part of the axial energy of the beam is converted into transverse energy. The axial velocity of the beam will then decrease accordingly.

To show this quantitatively, it can be shown that the transverse energy of a beam of electrons is proportional to the square of the beam radius r ,

$$E_t = kr^2 eV_0, \quad (4.1)$$

where k is a constant. From the conservation of beam energy, the sum of transverse energy, E_t , and axial energy, E_a , is conserved. As a matter of

fact, it is equal to eV_0 . Thus

$$\frac{1}{2} mu^2 + kr^2 eV_0 = eV_0 \quad (4.2)$$

The axial velocity of the electron is then

$$u = u_0 \sqrt{1 - kr^2} \quad (4.3)$$

where u_0 is the unperturbed beam velocity ($u_0 = \sqrt{2\eta V_0}$). Define a normalized beam radius ρ as

$$\rho = \sqrt{kr^2} \quad ,$$

then Eq. 4.3 becomes

$$u = u_0 \sqrt{1 - \rho^2} \quad (4.4)$$

Under active coupling the beam radius grows and thus the axial velocity will decrease in accordance with Eq. 4.4. The variation of axial velocity with ρ is shown in Fig. 4.1. It can be seen that the small-signal analysis would be valid for a normalized beam radius up to about 0.4; beyond that, small-signal solutions will not describe the behavior of the electrons correctly. This shows that for high gain, and therefore high efficiency operation, the effects of variation of axial velocity have to be taken into account.

Due to the reduction in beam velocity, the orbital electrons will slip away from the quadrupole pump field. The exact amount of slip under a particular pump field structure can be found from the solution of the equations of motion. In general, one can find the phase slip due to the variation of axial velocity as follows.

From Eq. 4.3 one can find the lag in z (beam axis) for a given amount of velocity variation δu as

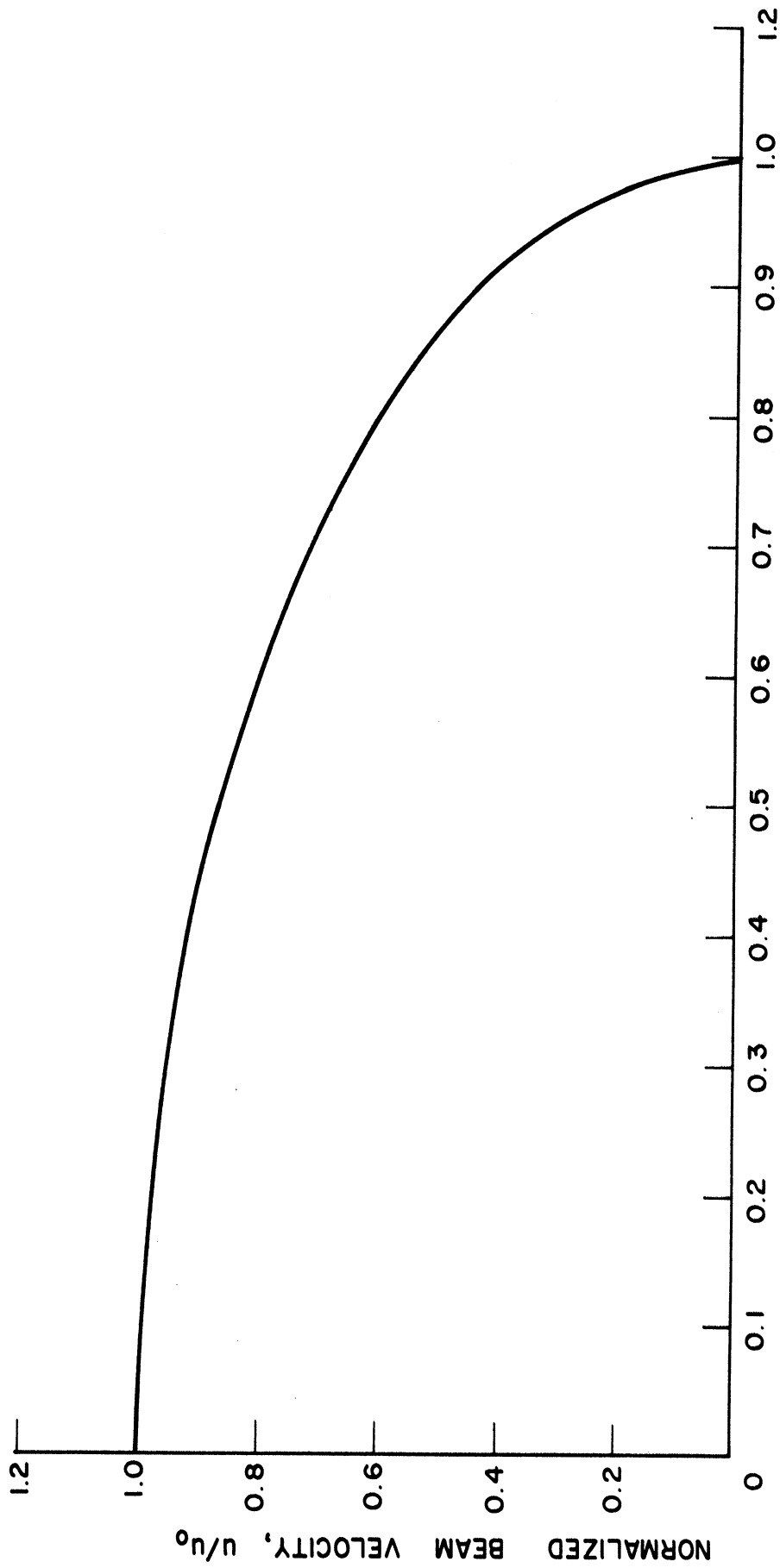


FIG. 4.1 NORMALIZED AXIAL BEAM VELOCITY u/u_0 VS. NORMALIZED BEAM RADIUS ρ .

$$\delta z = \delta t \delta u = (1 - \sqrt{1 - \rho^2}) u_0 \delta t , \quad (4.5)$$

where

$$\delta u = u_0 - u = u_0 [1 - \sqrt{1 - \rho^2}] . \quad (4.6)$$

The angular slip with respect to the pump field is then

$$\delta\phi = \beta_q \delta z , \quad (4.7)$$

where β_q is the propagation constant of the pump field structure. In the case of the quadrifilar helix quadrupole for cyclotron-synchronous wave amplification, the active coupling condition requires that the propagation constant of the signal be twice that of the pump structure, i. e., $\beta_c = 2\beta_q$. Under this condition, the phase lag with respect to the signal is

$$\begin{aligned} d\phi &= \frac{1}{2} \beta_c \delta z \\ &= \frac{1}{2} [1 - (1 - \rho^2)^{1/2}] d\tau , \end{aligned} \quad (4.8)$$

where $d\tau = \omega_c dt$.

As was shown in Quarterly Progress Report No. 3 (Eq. 4.47) the component wave as well as the beam radius grows with an exponential factor, γ , such that

$$\rho = \rho_0 e^{\gamma z} . \quad (4.9)$$

The propagation constant γ for cyclotron-synchronous wave interaction can be obtained as follows.

The potential distribution of the quadrifilar helix will be given by Eq. 4.21 later in this report. For cyclotron-synchronous wave

interaction, $\beta_q = 1/2\beta_c$, the distribution becomes

$$V(r, \theta, z) = V_p \frac{J_2(\beta_c r)}{J_2(\beta_c a)} \sin(2\theta - \beta_c z) .$$

The ratio of the Bessel functions can be approximated as

$$\frac{J_2(\beta_c r)}{J_2(\beta_c a)} \approx \frac{r^2}{a^2} .$$

The potential distribution expression is then reduced to

$$V(r, \theta, z) \approx \frac{V_p}{a^2} r^2 \sin(2\theta - \beta_c z) .$$

With this potential distribution, the equations of the polarized field in terms of the coupled modes can be written as

$$E_+ = - \frac{2V_p}{k\omega_c a^2} (a_4 - a_2) e^{j\beta_c z}$$

and

$$E_- = - \frac{2V_p}{k\omega_c a^2} (a_3 - a_1) e^{-j\beta_c z} ,$$

where k , a , a_1 , a_2 , a_3 and a_4 are the same as defined in Quarterly Progress Report No. 3. Following the same procedure the propagation constant γ_1 for the fast cyclotron wave is found to be

$$\gamma_1 = -j \frac{\beta_c}{2} + \sqrt{P - \frac{\beta_c^2}{4}} ,$$

where the pump parameter P is defined as

$$P = \frac{V_p}{u_0 \beta_c a^2} .$$

The gain constant γ for the fast cyclotron wave is the real part of γ_1 , which is

$$\gamma = \text{Re} [\gamma_1] = \sqrt{P - \frac{\beta_c^2}{4}} .$$

For a strong pump field condition, with $P \geq \beta_c^2/4$ and γ positive real, the gain constant is then

$$\gamma = \sqrt{P} = \sqrt{\frac{V_p}{u_0 \beta_c a^2}} .$$

In order to find the relationship between the phase slip and the variation of the beam radius, the following relations are used:

$$z = ut = \frac{u}{\omega_c} \tau$$

and

$$\begin{aligned} \rho &= \rho_0 e^{\gamma z} \\ &= \rho_0 e^{N \sqrt{1-\rho^2} \tau} , \end{aligned} \quad (4.10)$$

where $N = \gamma/\beta_c$.

Solving for τ in Eq. 4.10, one obtains

$$\tau = \frac{1}{N \sqrt{1-\rho^2}} \ln \frac{\rho}{\rho_0} \quad (4.11)$$

and

$$d\tau = \frac{1}{N(1-\rho^2)} \left[\frac{\sqrt{1-\rho^2}}{\rho} \frac{1}{\rho} + \frac{\rho}{\sqrt{1-\rho^2}} \ln \frac{\rho}{\rho_0} \right] d\rho . \quad (4.12)$$

Substitute $d\tau$ in Eq. 4.8 and obtain the variation in phase slip with respect to the signal as

$$d\phi = \frac{1}{2N(1-\rho^2)} [1 - (1 - \rho^2)^{1/2}] \left[\frac{1}{\rho} \sqrt{1 - \rho^2} + \frac{1}{\sqrt{1-\rho^2}} \rho \ln \frac{\rho}{\rho_0} \right] d\rho . \quad (4.13)$$

The total phase slip in time t can be obtained by integrating Eq. 4.13 with respect to ρ .

$$\begin{aligned} \phi &= \frac{1}{2} \int_{\rho_0}^{\rho} \frac{1}{N} [1 - \sqrt{1 - \rho^2}] \left[\frac{1}{\rho} \sqrt{1 - \rho^2} + \frac{1}{(1 - \rho^2)^{3/2}} \rho \ln \frac{\rho}{\rho_0} \right] d\rho \\ &= \frac{1}{2N} \left[- \ln \rho + \frac{1}{\sqrt{1 - \rho^2}} \ln \frac{\rho}{\rho_0} + \frac{1}{2} \ln (1 - \rho^2) \ln \frac{\rho}{\rho_0} + \frac{1}{4} \rho^2 \right]_{\rho_0}^{\rho} . \end{aligned} \quad (4.14)$$

Figure 4.2 shows the variation between the phase slip and the pump field strength. A line is drawn at a constant phase slip of 45 degrees, which serves as a boundary between the amplifying and attenuating phase. In other words electrons with a phase slip of greater than 45 degrees would fall into attenuating phase and will start giving up their rotational energy to the beam and eventually travel along the z-axis. This critical angle also defines the maximum useful beam radius for a given pump strength. Figure 4.3 shows the maximum beam radius for different pump field strengths. The exponential variation suggests that a high pump field operation is desirable. With a strong pump field (which is the required condition for the cyclotron-synchronous wave amplifier) a large rotating beam radius is permissible; this implies that an amplifier of this type can be operated at very high efficiency.

The effect of initial beam radius ρ_0 upon the phase slip is shown in Fig. 4.4. The curves indicate that larger initial beam radii will give better synchronism between the rotating beam and the pump field. However, the difference in phase slip over a wide variation of initial beam radii is not significantly large. For high gain operation, one would use a comparatively small input beam radius, and disregard this off-synchronous effect.

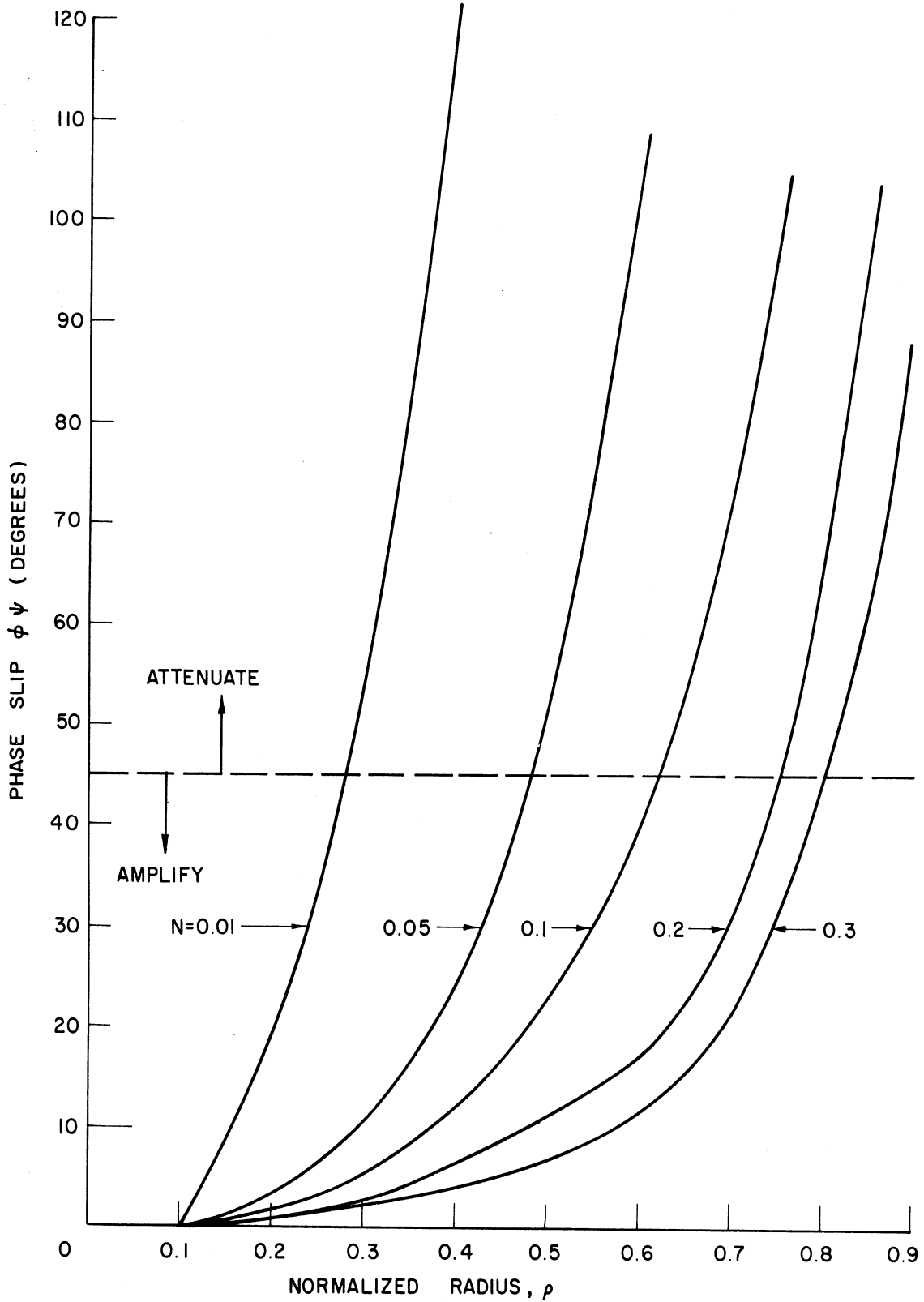


FIG. 4.2 PHASE SLIP VS. NORMALIZED BEAM RADIUS ρ WITH PUMP FIELD STRENGTH N AS PARAMETER.

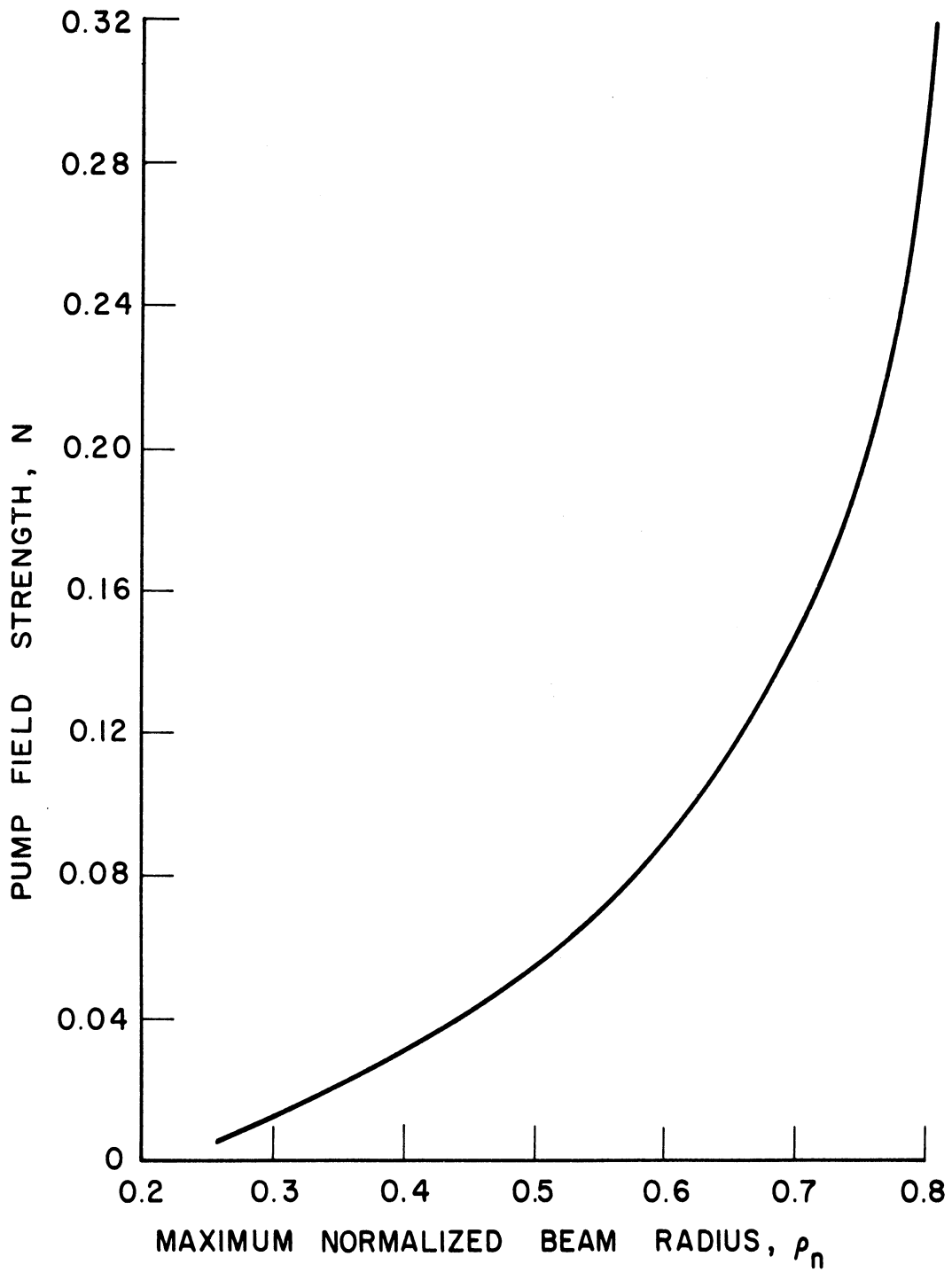


FIG. 4.3 PUMP FIELD STRENGTH N VS. MAXIMUM NORMALIZED BEAM RADIUS ρ_m .

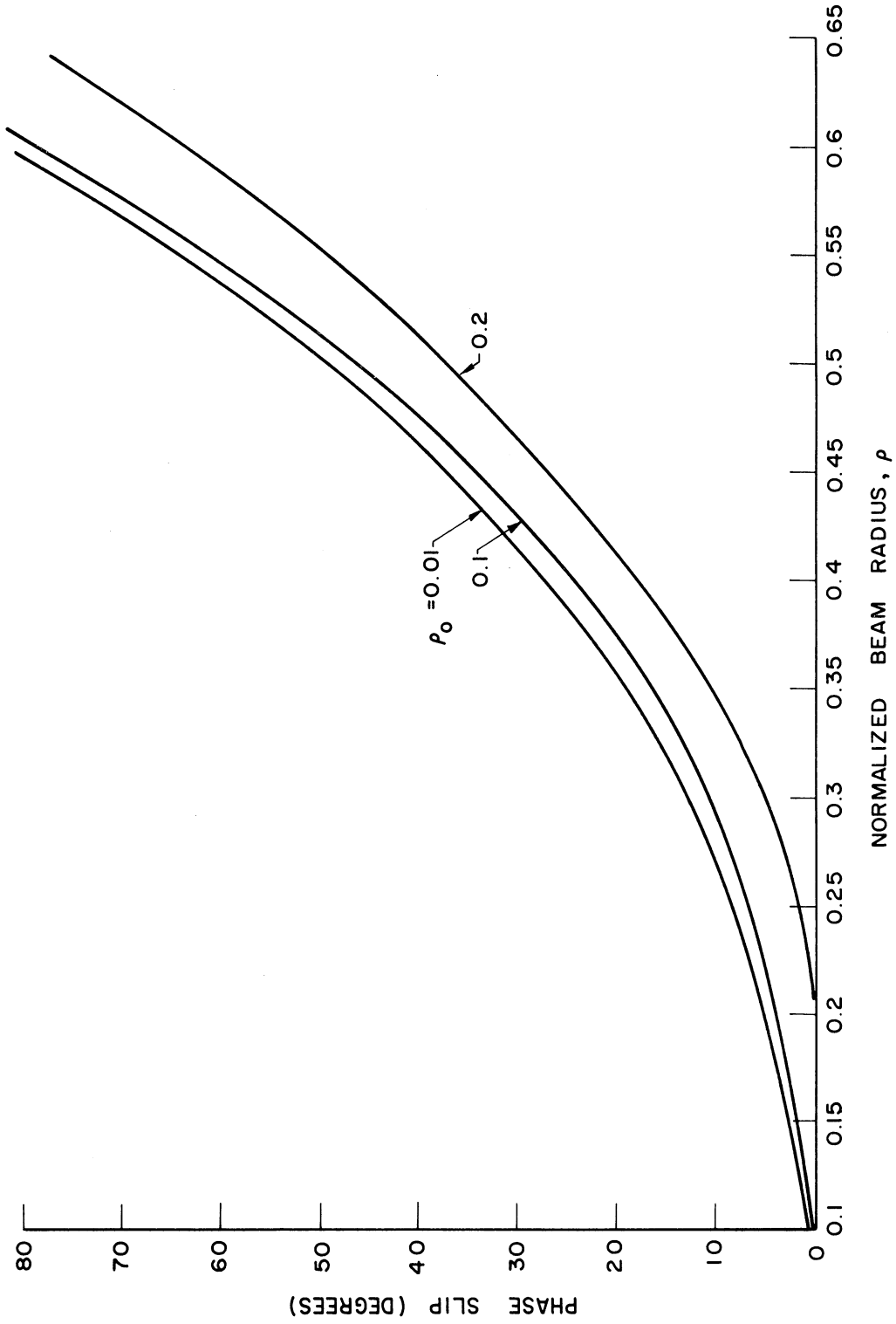


FIG. 4.4 PHASE SLIP VS. NORMALIZED BEAM RADIUS ρ WITH INITIAL BEAM RADIUS ρ_0 AS PARAMETER

PUMP FIELD STRENGTH $N = 0.05$.

4.2.3 Potential Distribution of the Pump Field. Since the trajectory of the electrons in the quadrupole region is determined by the potential distribution of the pump field an exact expression for the pump field is necessary for the large-signal analysis.

A quadrifilar helix is used for the pump field structure. For a cyclotron-synchronous wave amplifier the rate of the twist of the helices is half that of the electron beam, (i. e., $\lambda_q = 2\lambda_c$). The potential distribution can be obtained by solving Laplace's equation in cylindrical coordinates.

$$\frac{1}{r} \frac{\partial}{\partial r} \left(r \frac{\partial V}{\partial r} \right) + \frac{1}{r^2} \frac{\partial^2 V}{\partial \phi^2} + \frac{\partial^2 V}{\partial z^2} = 0 \quad (4.15)$$

with the boundary conditions

$$\begin{aligned} V &= 0 & \text{at } z &= 0 & \phi &= 0, \pi/2 \\ V &= V_p & \text{at } z &= 0 & \phi &= \pi/4 \\ V &= -V_p & \text{at } z &= 0 & \phi &= -\pi/4 \end{aligned} \quad (4.16)$$

A sinusoidal variation along the axial (z) direction is assumed. By the standard technique of separation of variables, the solution of the potential V is of the form

$$V(r, \phi, z) = A_{k_2} J_{k_2}(k_2 r) \sin(k_2 \phi - k_1 z) \quad , \quad (4.17)$$

where A_{k_2} is the amplitude coefficient and k_1 and k_2 are the parameters of separation for the $Z(z)$ and $\Phi(\phi)$ equations respectively.

The coefficients can be evaluated as follows:

1. For k_1 .

The periodicity in the axial direction should be half of the pitch of the helix due to the quadrature rotational symmetry of the structure.

Therefore, the coefficient, k_1 , should be

$$k_1 = 2\beta_q = \frac{4\pi}{p}, \quad (4.18)$$

where p is the pitch of the helix, and β_q is the propagation constant in the z -direction for the quadrupole pump field.

2. For k_2 .

The periodicity of the angular direction is π , which results from the polarity of the applied pump voltage. Then k_2 should have the value

$$k_2 = 2. \quad (4.19)$$

3. For A_{k_2} .

From the given boundary condition at the entrance plane ($z = 0$), the potential on the helix is

$$V = V_p \text{ at } \varphi = \pi/2, \quad r = a.$$

Equation 4.17 becomes

$$V_p = A_2 J_2 \left(\frac{4\pi}{p} a \right).$$

Therefore,

$$A_2 = \frac{V_p}{J_2(2\beta_q a)}. \quad (4.20)$$

The complete expression of the potential distribution of the quadrifilar helix field becomes

$$V(r, \varphi, z) = \frac{V_p}{J_2(2\beta_q a)} J_2(2\beta_q r) \sin(2\varphi - 2\beta_q z). \quad (4.21)$$

4.2.4 Equations of Motion. The equations of motion may now be written using the outlined assumptions and the above pump field expressions. In the previous report (No. 5) a set of equations for the cyclotron-cyclotron wave interaction was derived. Following the same formulation but using a different pump field condition one can obtain a set of equations for the cyclotron-synchronous wave interaction. They can be written in cylindrical coordinates as follows:

$$\begin{aligned} \ddot{r} - r(\dot{\theta})^2 + \omega_c r \dot{\theta} &= \eta \frac{V_p}{J(2\beta_q a)} \frac{\partial}{\partial r} J_2(2\beta_q r) \sin 2(\theta - \beta_q z) , \\ r\ddot{\theta} + 2\dot{r}\dot{\theta} - \omega_c \dot{r} &= 2\eta \frac{V_p}{rJ_2(2\beta_q a)} J_2(2\beta_q r) \cos 2(\theta - \beta_q z) , \\ \ddot{z} &= -2\eta\beta_q \frac{V_p}{J(2\beta_q a)} J_2(2\beta_q r) \cos 2(\theta - \beta_q z) . \end{aligned} \quad (4.22)$$

Introducing the transformation,

$$\varphi = \theta - \tau ,$$

and the change of variables,

$$\text{normalized radius } \rho = \beta_c r ,$$

$$\text{normalized axial displacement } \xi = \beta_c z ,$$

the equations of motion can then be written as

$$\begin{aligned} \frac{d^2\rho}{d\tau^2} - \rho \left(\frac{d\varphi}{d\tau} \right)^2 - \rho \frac{d\varphi}{d\tau} &= K \frac{\partial}{\partial \rho} J_2(\rho) \sin 2 \left(\varphi + \tau - \frac{1}{2} \xi \right) , \\ \frac{d^2\varphi}{d\tau^2} + \frac{2}{\rho} \frac{d\rho}{d\tau} \frac{d\varphi}{d\tau} + \frac{1}{\rho} \frac{d\rho}{d\tau} &= 2 K J_2(\rho) \cos 2 \left(\varphi + \tau - \frac{1}{2} \xi \right) , \\ \frac{d^2\xi}{d\tau^2} &= - K J_2(\rho) \cos 2 \left(\varphi + \tau - \frac{1}{2} \xi \right) , \end{aligned} \quad (4.23)$$

where $K = V_p / 2V_0 J_2(\beta_c a)$ is the pump field parameter for this interaction.

The solution for the normalized radius ρ , the normalized axial displacement ξ , and the angular displacement ϕ will describe the trajectory of the beam completely.

4.2.5 Energy Considerations. The study of the energy exchange between the cyclotron waves, beam and the pump field is an essential part of the analysis, from which one can obtain further insight into the interaction mechanism, especially when high efficiency operation is desired. From the equations of motion derived in Section 4.2.4, the energy equation can be obtained in the following manner.

Consider that an electron beam with no initial modulation travels in a uniform magnetic field so that the electrons of the beam would have an axial energy of $E_0 = eV_0$, where V_0 is the beam voltage. Suppose now that the beam is excited by a transverse electric field, the resultant transverse velocity can be resolved into two components, namely, the radial velocity v_R and tangential velocity v_T . By the use of the transformation $\phi = \theta - \tau$, the normalized radius ρ and time variable $\tau = \omega_c t$, these two velocity components can be expressed as

$$v_R = \frac{dr}{dt} = \frac{\omega_c}{\beta_c} \dot{\rho} \quad (4.24)$$

and

$$v_T = r \frac{d\theta}{dt} = \frac{\rho \omega_c}{\beta_c} (1 + \dot{\phi}) \quad (4.25)$$

Since energy is proportional to the square of velocity the transverse energy can be written as

$$E_{Tr} = E_0 \left(\frac{v}{u_0} \right)^2, \quad (4.26)$$

where E_0 is the d-c beam energy, eV_0 , and is also the maximum transverse energy a beam electron can possibly have. Under such a condition the axial energy is transferred completely into transverse energy. For any beam radius ρ , the radial component of the transverse energy is

$$E_R = E_0 \left(\frac{v_R}{u_0} \right)^2 = E_0 \left(\frac{\omega_c \dot{\rho}}{\beta_c u_0} \right)^2 = eV_0 \dot{\rho}^2 . \quad (4.27)$$

The tangential component of the transverse energy is

$$\begin{aligned} E_T &= E_0 \left[\frac{\rho \omega_c (1+\dot{\phi})}{\beta_c u_0} \right]^2 \\ &= eV_0 \rho^2 (1 + \dot{\phi})^2 . \end{aligned} \quad (4.28)$$

To obtain these transverse energy expressions from the equation of motion, proceed as follows.

In order to have $\dot{\rho}^2$ for the radial energy expression, multiply the radial equation of motion by $\dot{\rho}$ and then integrate with respect to τ so that

$$\dot{\rho}^2 - 2 \int [\rho \dot{\rho} \ddot{\phi}^2 + \rho \dot{\rho} \dot{\phi}] d\tau = 2 K J_2(\rho) \sin 2 \left(\phi + \tau - \frac{1}{2} \xi \right) + C_1 , \quad (4.29)$$

where C_1 is the integration constant. Next, to obtain the factor

$\rho^2(1 + \dot{\phi})^2$ in E_T , multiply the angular equation of motion by $\rho^2(1 + \dot{\phi})$ and integrate obtaining

$$\begin{aligned} \int \rho(\rho \ddot{\phi} + \dot{\rho})(1 + \dot{\phi}) d\tau + 2 \int [\rho \dot{\rho} \dot{\phi} + \rho \dot{\rho} \dot{\phi}^2] d\tau \\ = 2 K J_2(\rho) \sin 2 \left(\phi + \tau - \frac{1}{2} \xi \right) + C_2 . \end{aligned} \quad (4.30)$$

Again C_2 is the integration constant. Finally, multiply the axial equation of motion by $\dot{\xi}$ and integrate to obtain

$$\dot{\xi}^2 = 2 K J_2(\rho) \sin 2 \left(\phi + \tau - \frac{1}{2} \xi \right) + C_3 , \quad (4.31)$$

where C_3 relates the initial energy of the beam at the entrance of the pump field region. Summing Eqs. 4.29, 4.30, 4.31, and multiplying both sides by eV_0 , the energy equation is then obtained.

$$eV_0 \dot{\rho}^2 + eV_0 \rho^2 (1 + \dot{\phi})^2 + eV_0 \dot{\xi}^2 = 8 eV_0 K J_2(\rho) \sin 2(\varphi + \tau - \frac{1}{2} \xi) + C_4, \quad (4.32)$$

where

$$C_4 = C_1 + C_2 + C_3.$$

The interpretation of the left-hand side of Eq. 4.32 is now obvious. The first and second terms are exactly the radial and tangential transverse energy respectively as given by Eqs. 4.27 and 4.28 while the third term $eV_0 \dot{\xi}^2$ can be transformed into $1/2 m \dot{z}^2$, which is the axial energy of the beam electron. The constant C_4 can be evaluated as follows. At the entrance plane the initial values are

$$z = 0, \quad \dot{z} = u_0 \dot{\xi} = \left. \frac{d\xi}{d\tau} \right|_{\xi=0} = \frac{\beta_c}{\omega_c} \left. \frac{dz}{dt} \right|_{z=0} = 1$$

and

$$\xi = \varphi = \tau = \rho = \dot{\rho} = \dot{\phi} = 0.$$

From Eq. 4.32 one obtains

$$C_4 = eV_0.$$

Therefore, the energy equation becomes

$$\dot{\rho}^2 + \rho^2 (1 + \dot{\phi})^2 + \dot{\xi}^2 = 1 + 8 K J_2(\rho) \sin 2(\varphi + \tau - \frac{1}{2} \xi). \quad (4.33)$$

The interpretation of the right-hand side of the energy equation can now be made. The first term is the total normalized beam energy supplied by the collector of the tube. The second term then must be the energy supplied by the pump field. To be more exact, this term has a sinusoidal variation and indicates that there is a kind of energy exchange between the beam and the pump field. The interpretation of the energy equation can be summed up by the following expression:

$$E_R + E_T + E_A = E_B + E_P , \quad (4.34)$$

where E_R = radial energy,

E_T = tangential energy,

E_{rot} = rotation energy = $E_R + E_T$,

E_A = axial energy,

E_B = total beam energy and

E_P = energy supplied by the pump field.

The variation of these energy expressions is shown qualitatively in Fig. 4.5.

4.3 Future Work. The equations of motion and the energy relation derived in this report will be programmed to compute the beam trajectories. The results will be compared with the previous computation for cyclotron-cyclotron wave interaction to obtain further insight into the interaction mechanisms.

5. General Conclusions (C. Yeh)

Beryllium oxide is known to have a very high thermal conductivity, comparable to that for some metallic conductors. It has been used to support the helix structure of a traveling-wave tube in order to increase the

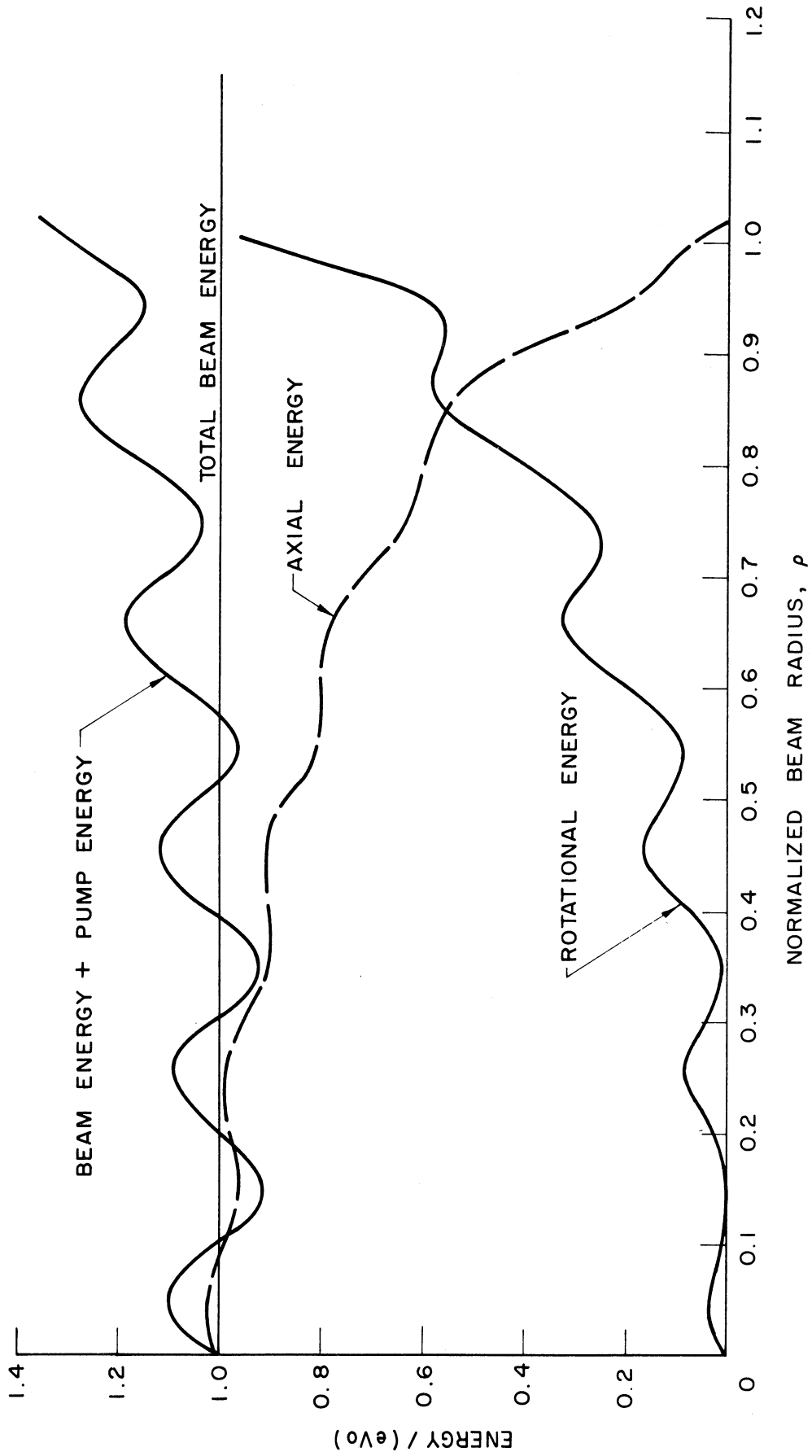


FIG. 4.5 ENERGY RELATIONS VS. NORMALIZED BEAM RADIUS.

heat dissipation capability. A proper method of loading the helix coil into the BeO tube is required to be sure of making perfect thermal contact. A scheme has been developed to achieve these objectives during the last period of work. It is confident now that an X-band helix circuit structure capable of dissipating 170 watts/inch along the helix at a mean temperature of 500°C or less can be constructed. Further developments may push the limit somewhat. It has been decided that this phase of work will terminate after final test runs to be conducted during the next reporting period. A final report concerning the effort and results of this investigation will be prepared in the next period.

A number of computational results have been obtained from the multi-signal analyses of the traveling-wave amplifier. Some illustrative examples are given in this report in the form of curves to illustrate the output of the amplitude- and phase-modulated TWA, the cross-modulation factor, etc. using different theories. Experimental checks with the theories are also illustrated and discussed. In general, the experimental results check reasonably well with the theories. Experimental results are given for the three input signal case. It is believed that the theory of cross modulation in traveling-wave amplifiers is well understood and the experimental results are satisfactory. A final report on this effort will be prepared during the next reporting period.

Large-signal analyses of a d-c pumped quadrupole amplifier involving a cyclotron-synchronous wave interaction mechanism have been performed. The resulting equations of motion will be programmed for computer study. Equations for the phase slip of the electron beam with respect to the applied pumping field resulting from the energy interchange between them are derived and studied. Phase slip is used as a criterion

for applying small- or large-signal analyses. Energy relations between the beam and the pumping field are discussed.

In view of the fact that two of the areas of investigation will be terminated during the next reporting period, two new areas of investigation will be initiated. These are the study of cross modulation in crossed-field amplifiers and a similar study of tunnel-diode amplifiers.

<u>No. Copies</u>	<u>Agency</u>
1	Microwave Electronics Corporation, 3165 Porter Drive, Stanford Industrial Park, Palo Alto, California
1	Mr. A. G. Peifer, Bendix Corporation, Research Laboratories, Northwestern Highway and 10-1/2 Mile Road, Southfield, Michigan
1	Bendix Corporation, Systems Division, 3300 Plymouth Road, Ann Arbor, Michigan, Attn: Technical Library
1	Litton Industries, 960 Industrial Road, San Carlos, California, Attn: Technical Library
1	Dr. R. P. Wadhwa, Electron Tube Division, Litton Industries, 960 Industrial Way, San Carlos, California
1	Microwave Associates, Burlington, Massachusetts, Attn: Technical Library
1	Microwave Electronic Tube Company, Inc., Salem, Massachusetts, Attn: Technical Library
1	Radio Corporation of America, Power Tube Division, Harrison, New Jersey
1	Raytheon Company, Burlington, Massachusetts, Attn: Technical Library
1	S-F-D Laboratories, 800 Rahway Avenue, Union, New Jersey, Attn: Technical Library
1	Dr. Walter M. Nunn, Jr., Electrical Engineering Department, Tulane University, New Orleans, Louisiana
1	Westinghouse Electric Corporation, P. O. Box 284, Elmira, New York, Attn: Technical Library
1	Bendix Corporation, Red Bank Division, Eatontown, New Jersey, Attn: Dr. James Palmer
1	Mr. A. Weglein, Hughes Aircraft Company, Microwave Tube Division, 11105 South LaCienaga Blvd., Los Angeles 9, California
1	The University of Arizona, University Library, Tucson, Arizona
1	Eitel-McCullough, Inc., 13259 Sherman Way, North Hollywood, California, Attn: Dr. John E. Nevins, Jr.

<p>DD</p> <p>The University of Michigan, Electron Physics Laboratory, Ann Arbor, Michigan. BASIC RESEARCH IN MICROWAVE DEVICES AND QUANTUM ELECTRONICS, by H. K. Detweiler, et al. November, 1964, 45 pp. Incl. illus. (Project Serial No. SRO06030L, Task 959L, Contract No. N0bsr-89274)</p> <p>Equations for the modulation products in the multi-signal analysis of an amplitude- and phase-modulated traveling-wave amplifier have been programmed and the results computed. The computation includes all three theoretical approaches derived and discussed in previous reports. These include the nonlinear approach using the two-signal input, the large-signal analysis using the multiple signal input and the Boltzmann transport equation approach using the multiple signal input. The output powers of some important cross-modulation components, the cross-modulation factors, etc. are presented in graphs. Experimental results using two and three signal inputs are presented for comparison.</p> <p>A large-signal analysis is carried out for a d-c pumped quadrupole amplifier employing cyclotron-to-synchronous wave interaction. Criteria for the validity of small-signal and large-signal analyses are established by means of the phase slip. Energy relations between the beam and the pumping field are discussed for a strong pumping field condition that would lead to the anomalous gain possibility.</p> <p>The technique for insertion of the helix-BeO rod into a metal envelope to improve the thermal conductivity of the assembly is developed.</p>	<p>UNCLASSIFIED</p> <ol style="list-style-type: none"> 1. General Introduction. 2. Generation and Amplification of Coherent Electromagnetic Energy in the Millimeter and Submillimeter Wavelength Region. 3. Analysis of Amplitude- and Phase-Modulated Traveling-Wave Amplifiers. 4. Study of a D-c Pumped Quadrupole Amplifier. 5. General Conclusions. I. Detweiler, H. K. II. El-Shandawily, M. E. III. Ho, B. IV. Rowe, J. E. V. Yeh, C. 	<p>UNCLASSIFIED</p> <ol style="list-style-type: none"> 1. General Introduction. 2. Generation and Amplification of Coherent Electromagnetic Energy in the Millimeter and Submillimeter Wavelength Region. 3. Analysis of Amplitude- and Phase-Modulated Traveling-Wave Amplifiers. 4. Study of a D-c Pumped Quadrupole Amplifier. 5. General Conclusions. I. Detweiler, H. K. II. El-Shandawily, M. E. III. Ho, B. IV. Rowe, J. E. V. Yeh, C.
<p>DD</p> <p>The University of Michigan, Electron Physics Laboratory, Ann Arbor, Michigan. BASIC RESEARCH IN MICROWAVE DEVICES AND QUANTUM ELECTRONICS, by H. K. Detweiler, et al. November, 1964, 45 pp. Incl. illus. (Project Serial No. SRO06030L, Task 959L, Contract No. N0bsr-89274)</p> <p>Equations for the modulation products in the multi-signal analysis of an amplitude- and phase-modulated traveling-wave amplifier have been programmed and the results computed. The computation includes all three theoretical approaches derived and discussed in previous reports. These include the nonlinear approach using the two-signal input, the large-signal analysis using the multiple signal input and the Boltzmann transport equation approach using the multiple signal input. The output powers of some important cross-modulation components, the cross-modulation factors, etc. are presented in graphs. Experimental results using two and three signal inputs are presented for comparison.</p> <p>A large-signal analysis is carried out for a d-c pumped quadrupole amplifier employing cyclotron-to-synchronous wave interaction. Criteria for the validity of small-signal and large-signal analyses are established by means of the phase slip. Energy relations between the beam and the pumping field are discussed for a strong pumping field condition that would lead to the anomalous gain possibility.</p> <p>The technique for insertion of the helix-BeO rod into a metal envelope to improve the thermal conductivity of the assembly is developed.</p>	<p>UNCLASSIFIED</p> <ol style="list-style-type: none"> 1. General Introduction. 2. Generation and Amplification of Coherent Electromagnetic Energy in the Millimeter and Submillimeter Wavelength Region. 3. Analysis of Amplitude- and Phase-Modulated Traveling-Wave Amplifiers. 4. Study of a D-c Pumped Quadrupole Amplifier. 5. General Conclusions. I. Detweiler, H. K. II. El-Shandawily, M. E. III. Ho, B. IV. Rowe, J. E. V. Yeh, C. 	<p>UNCLASSIFIED</p> <ol style="list-style-type: none"> 1. General Introduction. 2. Generation and Amplification of Coherent Electromagnetic Energy in the Millimeter and Submillimeter Wavelength Region. 3. Analysis of Amplitude- and Phase-Modulated Traveling-Wave Amplifiers. 4. Study of a D-c Pumped Quadrupole Amplifier. 5. General Conclusions. I. Detweiler, H. K. II. El-Shandawily, M. E. III. Ho, B. IV. Rowe, J. E. V. Yeh, C.
<p>DD</p> <p>The University of Michigan, Electron Physics Laboratory, Ann Arbor, Michigan. BASIC RESEARCH IN MICROWAVE DEVICES AND QUANTUM ELECTRONICS, by H. K. Detweiler, et al. November, 1964, 45 pp. Incl. illus. (Project Serial No. SRO06030L, Task 959L, Contract No. N0bsr-89274)</p> <p>Equations for the modulation products in the multi-signal analysis of an amplitude- and phase-modulated traveling-wave amplifier have been programmed and the results computed. The computation includes all three theoretical approaches derived and discussed in previous reports. These include the nonlinear approach using the two-signal input, the large-signal analysis using the multiple signal input and the Boltzmann transport equation approach using the multiple signal input. The output powers of some important cross-modulation components, the cross-modulation factors, etc. are presented in graphs. Experimental results using two and three signal inputs are presented for comparison.</p> <p>A large-signal analysis is carried out for a d-c pumped quadrupole amplifier employing cyclotron-to-synchronous wave interaction. Criteria for the validity of small-signal and large-signal analyses are established by means of the phase slip. Energy relations between the beam and the pumping field are discussed for a strong pumping field condition that would lead to the anomalous gain possibility.</p> <p>The technique for insertion of the helix-BeO rod into a metal envelope to improve the thermal conductivity of the assembly is developed.</p>	<p>UNCLASSIFIED</p> <ol style="list-style-type: none"> 1. General Introduction. 2. Generation and Amplification of Coherent Electromagnetic Energy in the Millimeter and Submillimeter Wavelength Region. 3. Analysis of Amplitude- and Phase-Modulated Traveling-Wave Amplifiers. 4. Study of a D-c Pumped Quadrupole Amplifier. 5. General Conclusions. I. Detweiler, H. K. II. El-Shandawily, M. E. III. Ho, B. IV. Rowe, J. E. V. Yeh, C. 	<p>UNCLASSIFIED</p> <ol style="list-style-type: none"> 1. General Introduction. 2. Generation and Amplification of Coherent Electromagnetic Energy in the Millimeter and Submillimeter Wavelength Region. 3. Analysis of Amplitude- and Phase-Modulated Traveling-Wave Amplifiers. 4. Study of a D-c Pumped Quadrupole Amplifier. 5. General Conclusions. I. Detweiler, H. K. II. El-Shandawily, M. E. III. Ho, B. IV. Rowe, J. E. V. Yeh, C.

UNIVERSITY OF MICHIGAN



3 9015 02519 6166